THE ASTROPHYSICAL JOURNAL, 591:891–915, 2003 July 10

CHANDRA X-RAY SPECTROSCOPIC IMAGING OF SAGITTARIUS A* AND THE CENTRAL PARSEC OF THE GALAXY

F. K. BAGANOFF,[1] Y. MAEDA,[2] M. MORRIS,[3] M. W. BAUTZ,[1] W. N. BRANDT,[4] W. CUI,[5] J. P. DOTY,[1] E. D. FEIGELSON,[4] G. P. GARMIRE,[4] S. H. PRAVDO,[6] G. R. RICKER,[1] AND L. K. TOWNSLEY[4]

Received 2001 February 2; accepted 2003 February 28

ABSTRACT

We report the results of the first-epoch observation with the ACIS-I instrument on the *Chandra X-Ray Observatory* of Sagittarius A* (Sgr A*), the compact radio source associated with the supermassive black hole (SMBH) at the dynamical center of the Milky Way. This observation produced the first X-ray (0.5–7 keV) spectroscopic image with arcsecond resolution of the central $17' \times 17'$ (40 pc $\times$ 40 pc) of the Galaxy. We report the discovery of an X-ray source, CXOGC J174540.0−290027, coincident with Sgr A* within $0\farcs27 \pm 0\farcs18$. The probability of a false match is estimated to be $\lesssim 0.5\%$. The spectrum is well fitted either by an absorbed power law with photon index $\Gamma \approx 2.7$ or by an absorbed optically thin thermal plasma with $kT \approx 1.9$ keV and column density $N_{\rm H} \approx 1 \times 10^{23}$ cm^{-2}. The observed flux in the 2–10 keV band is $\approx 1.3 \times 10^{-13}$ ergs cm^{-2} s^{-1}, and the absorption-corrected luminosity is $\approx 2.4 \times 10^{33}$ ergs s^{-1}. The X-ray emission at the position of Sgr A* is extended, with an intrinsic size of $\approx 1\farcs4$ (FWHM), consistent with the Bondi accretion radius for a $2.6 \times 10^6\ M_\odot$ black hole. A compact component within the source flared by up to a factor of 3 over a period of $\approx$1 hr at the start of the observation. The search for Kα line emission from iron was inconclusive, yielding an upper limit on the equivalent width of 2.2 keV. Several potential stellar origins for the X-ray emission at Sgr A* are considered, but we conclude that the various properties of the source favor accretion onto the SMBH as the origin for the bulk of the emission. These data are inconsistent with "standard" advection-dominated accretion flow (ADAF) models or Bondi models, unless the accretion rate from stellar winds is much lower than anticipated. The central parsec of the Galaxy contains an $\approx$1.3 keV plasma with electron density $n_e \approx 26\eta_f^{-1/2}$cm^{-3}, where η_f is the filling factor. This plasma should supply $\approx 10^{-6}\ M_\odot$ yr^{-1} of material to the accretion flow at the Bondi radius, whereas measurements of linear polarization at 150 GHz and above limit the accretion rate near the event horizon to $\lesssim 10^{-8}\ M_\odot$ yr^{-1}, assuming an equipartition magnetic field. Taken together, the X-ray and radio results imply that outflows or convection are playing a role in ADAF models and subequipartition magnetic fields in Bondi models, or else the X-ray emission must be generated predominantly via the synchrotron self-Compton (SSC) process. The measured extent of the source and the detection of short timescale variability are evidence that the emission from Sgr A* contains *both* thermal and nonthermal emission components at comparable levels. We also discuss the complex structure of the X-ray emission from the Sgr A radio complex and along the Galactic plane. Morphological evidence is presented that Sgr A* and the H II region Sgr A West lie within the hot plasma in the central cavity of Sgr A East, which we interpret as a supernova remnant that may have passed through the position of the SMBH, leading to a period of increased activity that ended within the past $\approx$300 yr. Similarly, we have discovered bright clumps of X-ray emission located on opposite sides of the Galactic plane, along a line passing through the central parsec of the Galaxy. The arrangement of these lobes suggests that Sgr A* may have experienced an earlier period of increased activity lasting several thousand years during which it expelled hot gas in a bipolar outflow oriented roughly perpendicular to the Galactic plane. Additionally, we present an analysis of stellar emission within the central parsec of the Galaxy.

Subject headings: accretion, accretion disks — black hole physics — galaxies: active — Galaxy: center — X-rays: ISM — X-rays: stars

1. INTRODUCTION

After decades of controversy, measurements of stellar dynamics have confidently established that the nucleus of the Milky Way harbors a supermassive black hole (SMBH) with a mass $M \approx 2.6 \times 10^6\ M_\odot$ (Genzel et al. 1997, 2000; Ghez et al. 1998, 2000; Schödel et al. 2002). The SMBH coincides with the compact nonthermal radio source Sagittarius A* (Sgr A*), but no emission at other wavelengths has been convincingly associated with it (§ 2.1). It is also well known that the bolometric luminosity (L) and the X-ray luminosity ($L_{\rm X}$) of Sgr A* are far lower than expected from the standard thin accretion disk model used in the study of X-ray binaries and quasars (Shakura & Sunyaev 1973; Watson et al. 1981; Bradt & McClintock 1983; Frank, King, & Raine 1992; Morris & Serabyn 1996 and references therein). The bolometric luminosity of a $2.6 \times 10^6\ M_\odot$ black hole radiating at the Eddington rate ($L_{\rm E}$) is $\sim 3 \times 10^{44}$ ergs s^{-1}, while the measured bolometric luminosity of Sgr A* is $\lesssim 10^{37}$ ergs s^{-1} (see Narayan et al. 1998a and references

[1] Center for Space Research, Massachusetts Institute of Technology, Cambridge, MA 02139-4307; fkb@space.mit.edu.
[2] Institute of Space and Astronautical Science, 3-1-1 Yoshinodai, Sagamihara 229-8501, Japan.
[3] Department of Physics and Astronomy, University of California, Los Angeles, CA 90095-1562.
[4] Department of Astronomy and Astrophysics, Pennsylvania State University, University Park, PA 16802-6305.
[5] Department of Physics, Purdue University, West Lafayette, IN 47907.
[6] Jet Propulsion Laboratory, California Institute of Technology, Pasadena, CA 91109.

therein). In the standard model, ~10% of the luminosity is in X-rays (Frank et al. 1992), so one would expect $L_X \sim 3 \times 10^{43}$ ergs s^{-1} if Sgr A* were radiating at the Eddington rate. The SMBH at Sgr A* has been undetected in the 2–10 keV band with $L_X < 10^{35}$ ergs s^{-1} (§ 2.2), which is $\sim 10^9$ times fainter than the X-ray luminosity that would be expected at the Eddington rate. Similarly, the $\sim 10^6$ $M_\odot$ SMBHs at the cores of several nearby spiral galaxies emit $L_X \simeq 10^{37}$–10^{39} ergs s^{-1}, implying that they are $\sim 10^5$–10^7 times fainter in X-rays than would be expected at their Eddington rates (Garcia et al. 2000; Terashima, Ho, & Ptak 2000; Ho et al. 2001).

The absence of a strong, compact X-ray source associated with the SMBH at the Galactic center has been one of the profound mysteries of high-energy astrophysics and must have at least one of three basic causes. First, the SMBH may reside in an environment where the accretion rate $\dot{M} \ll \dot{M}_E = L_E/(\eta_r c^2) \simeq 5.8 \times 10^{-3} \eta_r^{-1}$ $M_\odot$ yr^{-1}, either because the ambient gas has extremely low density, because it is too hot or is moving too fast to accrete efficiently, or because it is dynamically ejected prior to accretion. Here $\eta_r = L/(\dot{M}c^2)$ is the radiative efficiency of the accretion flow and c is the speed of light. Second, the mechanism of accretion may be such that the radiative efficiency is extremely low. The advection-dominated accretion flow (ADAF; Narayan, Mahadevan, & Quataert 1998b) and related models can achieve low values of η_r and have been intensively applied to the Sgr A* problem. Third, the X-ray emission from Sgr A* may be much higher than observed because of anisotropy (e.g., a relativistic beam oriented perpendicular to the Galactic plane) and/or extremely high absorption along the line of sight.

The *Chandra X-Ray Observatory* (*CXO*; Weisskopf et al. 1996), with its Advanced Charge-Coupled Device Imaging Spectrometer (ACIS; G. P. Garmire, J. P. Nousek, & M. W. Bautz, in preparation), provides a unique opportunity to advance our knowledge of X-ray emission from Sgr A*. It combines a mirror with subarcsecond resolution and an imaging detector with high efficiency over a broad energy band and moderate spectral resolution. The spatial resolution and accurate astrometry are essential to discriminate the emission of Sgr A* from that produced in the surrounding compact cluster of massive stars and hot plasma in the region. The sensitivity of *Chandra*/ACIS at energies above 2 keV is essential to penetrate the high interstellar absorbing column along the line of sight to the Galactic center (§ 2.1).

The central black hole of our Galaxy sits amid a complex of X-ray–emitting and absorbing entities, which complicates the analysis of the emission ascribable to Sgr A* but also provides a significant bonus in terms of the science that can be extracted from a single pointing with ACIS. In the immediate vicinity of Sgr A* lies a cluster of luminous young stars, many of which are windy emission-line stars that presumably supply the matter which the black hole is presently accreting (Krabbe et al. 1995; Blum, Sellgren, & DePoy 1996; Najarro et al. 1997; Coker & Melia 1997; Quataert, Narayan, & Reid 1999b; Paumard et al. 2001). These stars and their colliding winds are themselves potential X-ray sources (Ozernoy, Genzel, & Usov 1997). This cluster excites a parsec-scale H II region, Sgr A West, that is well studied at radio and infrared wavelengths. Surrounding Sgr A West is the dense, predominantly neutral circumnuclear disk (Morris & Serabyn 1996 and references therein). Beyond that, on a scale of ~10 pc, the nonthermal radio shell source Sgr A East surrounds the circumnuclear disk in projection. In a separate study (Maeda et al. 2002), we have interpreted Sgr A East—a strong X-ray source—as a supernova remnant. Figure 1 diagrams the relative placement of these structures.

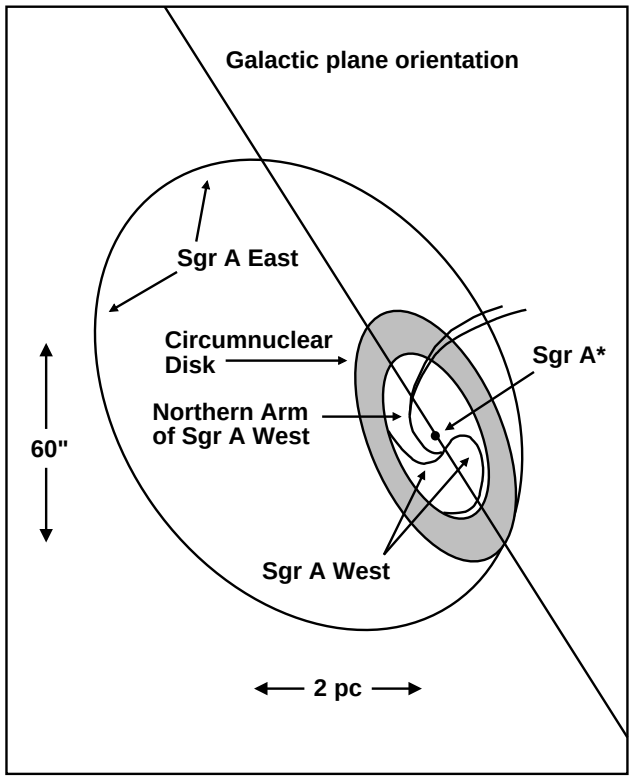

FIG. 1.—Schematic diagram of the principle constituents of the Sgr A radio complex, showing the previously known features discussed in this paper. The outer ellipse depicts the location of the radio shell of Sgr A East, which is a filled-center structure in X-rays (the red region in Fig. 2, and the yellow and green region on the left side of the central structure in Fig. 3). The circumnuclear disk, which is not evident in the X-ray maps, may affect the morphology of the X-ray–emitting region (see Fig. 4). The black hole candidate, Sgr A*, lies at the center of a cavity surrounded by the circumnuclear disk. The ionized gas features of Sgr A West and the central cluster of luminous, hot stars also lie within this cavity.

After a review of some relevant past studies (§ 2), we describe the observations, data analysis, source detection, and astrometry (§ 3). The resulting image of the inner 40 pc × 40 pc (17′ × 17′) of the Galaxy is presented in § 4, and the properties of the innermost arcsecond associated with Sgr A* are described in § 5. The integrated emission from stellar sources (§ 6) and the diffuse emission (§ 7) within the central 10″ of the Galaxy are discussed. Tentative identifications of discrete X-ray sources in the central 10″ with bright IR sources and the effects of source confusion on observations by other X-ray satellites are presented in § 6. The origin of the X-ray emission at Sgr A* (i.e., SMBH vs. stellar) is discussed (§ 8) and implications for the astrophysics of accretion onto the central SMBH of the Galaxy are presented (§ 9). We summarize our findings, evaluate the various models, and discuss the scientific goals of future observations in § 10. This is one of several papers arising from this *Chandra* observation. Future papers will present our studies of the X-ray emission from the point sources and the diffuse plasma distributed throughout the field.

2. PAST STUDIES

2.1. *Radio/IR*

Sgr A* is a compact, nonthermal radio source (Balick & Brown 1974; Backer 1996). Radio proper motion studies performed over the last decade place Sgr A* at the dynamical center of the Galaxy, and set a lower limit on its mass of $2 \times 10^4\ M_\odot$ (Backer & Sramek 1999; Reid et al. 1999). It has an intrinsic radio brightness temperature $\gtrsim 10^{10}$ K (Backer et al. 1993; Rogers et al. 1994), and is weakly variable on timescales of less than about a month in the centimeter and millimeter bands (Zhao 1989; Wright & Backer 1993; Falcke 1999; Tsuboi, Miyazaki, & Tsutsumi 1999; Zhao, Bower, & Goss 2001). These properties are reminiscent of the compact nuclear radio sources present in radio-loud quasars and active galactic nuclei (AGN) and suggest that Sgr A* may derive its luminosity from matter accreting onto the SMBH at the center of the Galaxy (Lynden-Bell & Rees 1971).

Polarimetric and spectropolarimetric observations made with the Very Large Array (VLA) and the Berkeley-Illinois-Maryland-Association (BIMA) radio interferometers show that Sgr A* is linearly unpolarized at frequencies up to 112 GHz (Bower et al. 1999a, 1999c, 2001); the upper-limit on linear polarization at 112 GHz is 1.8%. Aitken et al. (2000) report the detection of linear polarization from Sgr A* at 750, 850, 1350, and 2000 μm with the SCUBA camera on the 15 m James Clerk Maxwell Telescope (JCMT). After removing the effects of strong free-free emission and polarized dust from the single-dish JCMT beam (34″ at 150 GHz), they found that the fractional linear polarization at 2000 μm (150 GHz) is 10^{+9}_{-4}%, and that it increases with frequency. This result has recently been confirmed by Bower et al. (2003) using higher angular resolution observations with the BIMA array.

Circular polarization of Sgr A* has been detected at 1.4 to 14.9 GHz with the VLA (Bower, Falcke, & Backer 1999b) and the Australia Telescope Compact Array (ATCA; Bower et al. 2002). The fractional circular polarization at 4.8 GHz is $-0.37\% \pm 0.04\%$. The circular polarization at 4.8 GHz is confirmed independently by Sault & Macquart (1999) with the ATCA.

The total radio luminosity of Sgr A* is estimated to be a few hundred $L_\odot$ (Morris & Serabyn 1996). This raises the possibility that the emission could result from accretion onto a cluster of compact stellar-mass objects (Ozernoy 1989; Morris 1993). However, recent proper motion studies of stars within 6″ of the Galactic center constrain the minimum mass density of the central gravitational potential to be $\gtrsim 10^{12}\ M_\odot\ \mathrm{pc}^{-3}$ (Eckart & Genzel 1997; Ghez et al. 1998). The best-fit model from Ghez et al. requires a dark central object of mass $M = (2.6 \pm 0.2) \times 10^6\ M_\odot$ within $\sim$0.015 pc of Sgr A* (see also Genzel et al. 2000). These results rule out a cluster of compact stellar-mass objects as the energy source for Sgr A* (see Maoz 1998) but provide no direct evidence that the central engine is a SMBH. Furthermore, dynamical studies cannot provide the spectral information needed to identify the underlying emission mechanism or mechanisms.

Numerous models have been proposed that can produce centimeter- through millimeter-band spectra that are at least roughly consistent with the observations, but this spectral range is too narrow to identify uniquely the nature of the central engine. What is needed is a detection or strict upper limit on the flux of Sgr A* at higher frequencies to fix the overall spectrum on both ends.

Several claims have been made in the literature for the detection of Sgr A* in the mid- and near-IR (e.g., Stolovy, Hayward, & Herter 1996; Genzel et al. 1997). However, the search for an infrared (IR) counterpart to Sgr A* is hampered by source confusion and the strong IR background in the Galactic center. Precise astrometric alignment of IR images with radio maps using OH/IR stars that are also masers indicates that none of the confirmed IR sources seen so far can be associated definitively with the position of Sgr A* (Menten et al. 1997). Furthermore, none of the near-IR sources yet stands out spectroscopically as a possibly nonstellar object. Consequently, claims of detection of IR emission from Sgr A* are widely viewed as upper limits at this time.

The Galactic center is heavily obscured by gas and dust in the optical and ultraviolet wavebands ($A_V \sim 30$ mag) (Becklin et al. 1978; Rieke, Rieke, & Paul 1989). Thirty magnitudes of visual extinction corresponds to a column density $N_{\mathrm{H}} \approx 6 \times 10^{22}\ \mathrm{cm}^{-2}$ (Predehl & Schmitt 1995), so the obscuring medium becomes partially transparent to X-rays from the Galactic center at energies $\gtrsim 2$ keV. X-ray observations thus provide our best opportunity to constrain the high-frequency end of the spectral energy distribution of Sgr A*. Since strong, hard X-ray emission is a characteristic property of AGNs, Sgr A* is expected to be an X-ray source if it derives its energy from accretion onto a supermassive black hole. However, no definitive detection of X-ray emission from Sgr A* had been made prior to the launch of *Chandra* in 1999 July.

2.2. *X-Ray*

The earliest X-ray observations of the regions surrounding Sgr A* were carried out with rocket- and balloon-borne instruments (see review by Skinner 1989), but detailed observations started with *Einstein*, the first satellite equipped with grazing-incidence X-ray optics (Watson et al. 1981). *Einstein* observed the Galactic center twice, 6 months apart, with the IPC (0.5–4.0 keV) for a total of 18.3 ks and once with the HRI (0.5–4.5 keV) for 9.1 ks. The IPC images had an angular resolution of $\sim$1′ (FWHM) and revealed 12 discrete sources within the central $1^\circ \times 1^\circ$ of the Galaxy. The error box for the strongest of these sources, 1E 1742.5−2859, was centered only 20″ from the position of Sgr A*. Assuming an absorbed thermal bremsstrahlung model with $kT = 5$ keV and $N_{\mathrm{H}} = 6 \times 10^{22}\ \mathrm{cm}^{-2}$, Watson et al. estimated the absorption-corrected 0.5–4.5 keV luminosity of this source to be 9.6×10^{34} ergs s^{-1}.[7] The *Einstein* images showed that the discrete sources were embedded in a bright, 25′ × 15′ elliptically shaped region of apparently diffuse emission lying along the Galactic plane, which accounted for 85% of all the emission from that region. No variability was detected in the point sources over the 6 month baseline. The HRI image was essentially blank because of the high absorbing column and the low detection efficiency of that instrument.

Hard X-ray observations were made with 3′–5′ resolution in the late 1980s and early 1990s using *Spacelab-2*/XRT

[7] Throughout this paper we adopt 8.0 kpc for the distance from Earth to the center of our Galaxy (Reid 1993). All luminosities have been adjusted to this distance, except where specified otherwise.

(Skinner et al. 1987), *Spartan-1* (Kawai et al. 1988), and *Granat*/ART-P (Sunyaev, Markevitch, & Pavlinsky 1993; Pavlinsky, Grebenev, & Sunyaev 1994). The line of sight to the Galactic center becomes optically thin to X-rays with energies above a few keV; hence the fluxes measured by these missions were nearly free from the effects of absorption. These observations suggested the presence of a long-term variable source near the position of Sgr A* with an average 4–20 keV luminosity of $\sim 10^{36}$ ergs s^{-1}.

Prior to *Chandra*, the highest angular resolution observations were made with the PSPC and the HRI instruments on *ROSAT* (Predehl & Trümper 1994; Predehl & Zinnecker 1996). The PSPC observed the Galactic center for 50 ks in 1992 March and detected 14 sources within the central $30' \times 30'$ of the Galaxy. With the relatively high spatial resolution of 10″–20″, it resolved 1E 1742.5−2859 into three sources, of which RX J1745.6−2900 was coincident within 10″ with the radio position of Sgr A*. The high absorbing column combined with the soft energy band (0.1–2.5 keV) and modest spectral resolution of the PSPC limited its ability to constrain the parameters of the spectral fit. Following Watson et al., Predehl & Trümper adopted a thermal bremsstrahlung model with $kT = 5$ keV, but with $N_{\rm H} = 1.5 \times 10^{23}$ cm^{-2} to obtain broadband agreement with the hard X-ray data described above, and derived an unabsorbed 0.8–2.5 keV luminosity of 6.6×10^{35} ergs s^{-1} for the source.[8] The HRI, with $\sim 5''$ resolution and lower sensitivity than the PSPC, did not detect a source at the position of Sgr A* in a 27 ks exposure.

The first X-ray imaging of the Galactic center with charge-coupled devices (CCDs) was made in 1993 with *ASCA* (Koyama et al. 1996). The angular resolution of the *ASCA* mirrors was $\sim 1'$. *ASCA* detected diffuse thermal emission ($kT \approx 10$ keV) with helium-like and hydrogen-like Kα emission lines of various elements covering the central square degree of the Galaxy. A $2' \times 3'$ elliptical region filling the Sgr A East shell showed bright diffuse emission at a level 5 times that of the more extended emission. After correction for a measured absorption of $N_{\rm H} \approx 7 \times 10^{22}$ cm^{-2}, the unabsorbed 2–10 keV luminosity of this gas was found to be $\sim 10^{36}$ ergs s^{-1}. No subtraction was performed for the spatially variable local background, and consequently *ASCA* could only place an upper limit of $\sim 10^{36}$ ergs s^{-1} on the X-ray luminosity of Sgr A*. *ASCA* detected fluorescent line emission from cold iron in the molecular cloud Sgr B2 but could not find a bright X-ray irradiator nearby. This lead Koyama et al. to propose that the X-ray luminosity of Sgr A* some 300 yr ago may have been $\sim 3 \times 10^{39}$ ergs s^{-1}.

[8] Using the same data as Predehl & Trümper (1994), Predehl & Zinnecker (1996) reported the 0.8–2.5 keV luminosity of RX J1745.6−2900 as $(1–2) \times 10^{34}$ ergs s^{-1}, assuming an absorbed power-law model with $\Gamma = 1.6$ and $N_{\rm H} = 2 \times 10^{23}$ cm^{-2}. However, they did not specify whether this luminosity was corrected for absorption. We used the spectral model of Predehl & Zinnecker with the response matrix *pspcb_gain2_256.rsp* to compute the predicted PSPC count rate. Normalizing the model to the count rate observed by Predehl & Trümper (8×10^{-4} counts s^{-1}), we found that the luminosity reported by Predehl & Zinnecker had not been corrected for absorption. Several papers in the literature have used the luminosity reported by Predehl & Zinnecker under the assumption that it was unabsorbed (e.g., Melia & Falcke 2001). Consequently, the accretion models in these papers, which were based in part on fits to the luminosity reported by Predehl & Zinnecker, underestimated the upper limits on the accretion rate and the X-ray luminosity of Sgr A* in 1992 by 1–2 orders of magnitude.

Koyama et al. (1996) found a hard X-ray source located 1.′3 away from Sgr A*. During their second observation made in 1994, Maeda et al. (1996) discovered an X-ray burst and eclipses with a period of 8.4 hr from the hard source, establishing that it was an eclipsing low-mass X-ray binary (LMXB). Only one cataloged transient source, A 1742−289 (Eyles et al. 1975), which appeared in 1975, positionally coincides within the error region. However, Kennea & Skinner (1996) reanalyzed *Ariel V* data taken in 1975 and found no eclipses from A 1742−289. Hence, the hard source was identified as a newly discovered LMXB and given the name AX J1745.6−2901. Maeda et al. reported that the absorbed flux from this source varied from 1×10^{-11} to 4×10^{-11} ergs cm^{-2} s^{-1}, which was similar to the variations reported previously by the lower resolution hard X-ray instruments. Hence, the hard X-ray fluxes attributed to Sgr A* may have been contaminated significantly by AX J1745.6−2901 and A 1742−289 (see also Beckert et al. 1996).

A *BeppoSAX*/MECS observation, with on-axis angular resolution of $\sim 1.'3$ and an energy range similar to the *ASCA*/SIS, was performed in 1997 (Sidoli et al. 1999b). *BeppoSAX* detected the diffuse emission near Sgr A*, measured the absorption column to be $N_{\rm H} \approx 8 \times 10^{22}$ cm^{-2}, and set a tighter upper limit on the 2–10 keV luminosity of Sgr A* of $\lesssim 10^{35}$ ergs s^{-1}.

In the hard X-ray/soft gamma-ray band, observations with the SIGMA telescope on *Granat* yielded an upper limit of 6×10^{35} ergs s^{-1} (35–150 keV; Goldwurm et al. 1994). The EGRET instrument on the *Compton Gamma-Ray Observatory* (*CGRO*) detected a strong excess of emission from the Galactic center in the gamma-ray band (>30 MeV; Mayer-Hasselwander et al. 1998). The error-circle radius of 0.°2 included the position of Sgr A*. The source luminosity above 100 MeV was 2.2×10^{37} ergs s^{-1}. Mayer-Hasselwander et al. reported that the angular extent of the excess was only marginally consistent with that of a point source.

As we will see, most of the previously reported X-ray fluxes can be attributed to a combination of diffuse emission and numerous stellar sources lying within the instrumental resolution elements containing Sgr A*. The extremely low luminosity of Sgr A* and the detection of the multitude of other nearby sources reported here, indicate that this is in all likelihood the first true detection of X-ray emission from Sgr A*. No evidence exists at present that there have been any long-term variations of Sgr A* that would have allowed its detection with previous instruments (see § 5.4.2).

3. OBSERVATIONS AND ANALYSIS

3.1. *Data Acquisition and Reduction*

We observed the center of the Milky Way with *Chandra* for 51.1 ks on 1999 September 21. Detectors I0–I3 in the 2×2 element imaging array (ACIS-I) and detectors S2–S3 in the center of the 1×6 element spectroscopy array (ACIS-S) were read out. The photosensitive region of each CCD is comprised of 1024×1024 pixels, with each square pixel subtending 0.″492 on a side; hence, each CCD subtended $8.'3 \times 8.'3$ on the sky. Detector S3 is a backside-illuminated CCD; the other five are frontside-illuminated. The ACIS CCDs were clocked in timed-exposure (TE) mode using the standard integration time of 3.2 s per frame. The focal plane temperature was −110°C. To prevent telemetry saturation, events with energies $\gtrsim 15$ keV and events with ACIS flight

grade 24, 66, 106, 214, or 512 were rejected on orbit.[9] The data were telemetered to the ground in very faint (VF) mode; in this mode the telemetered data contains the pulse-height amplitudes (PHAs) of a 5×5 pixel island centered on each event.

The data were reduced using the *Chandra* Interactive Analysis of Observations (CIAO) software package. During ground processing, we further rejected events with *ASCA* grade 1, 5, or 7 and events with certain ACIS flight grades located on the CCD quadrant boundaries to minimize the quiescent instrumental background. Additional filtering was performed to exclude periods of time during which large background flares due to solar activity saturated the telemetry, causing the majority of frames in these intervals to be lost. The mean integrated count rates in S3 and the frontside-illuminated detectors were 4.12 ± 0.33 and 1.60 ± 0.09 counts s^{-1} CCD^{-1}, respectively. Events received during time intervals with count rates exceeding the mean count rate for that detector by more than 3.5 σ were removed from the event list. The total exposure time after filtering was 37.3 ks for S3 and 40.9 ks for each of the frontside-illuminated chips.

Analyses of on-orbit data by the *Chandra* X-Ray Center (CXC) and the ACIS Instrument Team have shown that the frontside-illuminated CCDs occasionally exhibit "flaring" pixels. This phenomenon occurs when a cosmic ray deposits a large amount of charge in traps at the interface between the active region and the insulating layer of the gate structure.[10] The detrapping time constant is longer than the integration time between frames, so events with identical grades are reported in the same pixel in up to 7 consecutive frames. These events can thus appear as false sources with $\lesssim 7$ counts. The CXC has developed an algorithm for removing these flaring pixel events. The current algorithm, however, removes a significant fraction of the events from real sources as well.[11] We have examined our source list (§ 3.2) and find that about 10% of the 158 sources have fewer than 8 counts, while 85% have at least 10 counts. Given the small number of potential flaring-pixel events, the expected number of flaring pixels that overlap with a real X-ray source within say 3″ is $\lesssim 0.06$. The key results of this paper (i.e., the astrometry and the spectral analyses) are based on sources with $\geqslant 10$ counts. These results will not be affected by flaring pixels, so we have therefore not filtered the data for flaring pixels.

Early in the *Chandra* mission, the frontside-illuminated CCDs suffered radiation damage believed to be caused by low-energy protons scattering off the high-resolution mirror assembly (HRMA) during repeated passages through Earth's radiation belts (Prigozhin et al. 2000). This radiation introduced charge traps in the buried channels of the CCDs that increased their charge transfer inefficiency (CTI). At the focal plane temperature of $-110°$C, the integrated spectrum of the five frontside-illuminated CCDs cuts off rapidly below ≈ 0.5 keV because of the increased CTI. In addition, the instrumental background begins to dominate the spectrum for energies $\gtrsim 7$–8 keV (e.g., Baganoff 1999; this paper). Therefore, the maximum signal-to-noise ratio for the integrated spectrum occurs in the energy range from about 0.5 to 7 keV. No attempt was made to correct the observed flight event grades for grade migration caused by the increased CTI. Event amplitudes were computed using the pulse heights from the central 3×3 pixels of each event.

An examination of the aspect solution file showed three discontinuities in the curves recording the position of the science instrument module (SIM) translation stage during the course of the observation. This problem was caused by warm pixels in the aspect camera that sometimes fell near one of the fiducial lights used to monitor the SIM drift. The amplitudes of the discontinuities were $\approx 0\farcs37$ along the Z-axis of the SIM and $\approx 0\farcs15$ along the Y-axis. The spacecraft roll angle was 268°.5, so the Z- and Y-axes were aligned nearly east-west and north-south, respectively. The source detection and spatial and variability analyses (§§ 3.2, 5.1, and 5.4) reported here were performed on the data after reprocessing by the CXC to correct the aspect solution and removing the 0″.5 pixel randomization introduced during the standard pipeline processing. All other analyses were performed on the uncorrected and randomized data.

3.2. *Source Detection and Astrometry*

We ran the wavelet source detection routine in CIAO (Freeman et al. 2002) on an image formed from events in the 0.5–7 keV band using kernel scales ranging from 1 to 16 pixels in multiples of $\sqrt{2}$. The source significance threshold was set equal to 1×10^{-7}. Since each CCD has about 1×10^6 pixels, the expected number of false detections in all six CCDs is about 0.6. The detection routine found 158 sources: 157 sources in I0–I3, 1 source in S2, and 0 sources in S3. The deficiency of sources in S2 and S3 is attributable to a combination of the mirror vignetting, the enlarged point-spread function (PSF) far off-axis ($\gtrsim 10\farcm3$), and the 2 times higher background rate in S3 compared to the frontside-illuminated devices. A detailed study of the point sources in the field will be presented in another paper.

The CXC has measured the on-orbit performance of the Pointing Control and Aspect Determination (PCAD) system on *Chandra* (see § 5.4 and Table 5.1 of the POG). Their analysis shows that standard pipeline processing is capable of placing a reconstructed X-ray image on the celestial sphere to an accuracy of 0″.76 (RMS) in radius. This corresponds to a projected distance of about 0.03 pc or 35 lt-days at the Galactic center. To improve on this, we reregistered the *Chandra* field using matching sources in the *Tycho-2* optical astrometric catalog from the *Hipparcos* satellite (Høg et al. 2000).

The center of our Galaxy is highly obscured (§ 2.1), so known optical sources in the field of view must be relatively close to Earth. The obscuring medium becomes partially transparent to X-rays from the Galactic center at energies above about 2 keV. Therefore, we applied the wavelet detection algorithm to a 0.5–1.5 keV image to select foreground X-ray sources. This yielded a total of 72 foreground sources in the field of view: 71 sources in I0–I3 and 1 source in S2.

To minimize any potential effects of the variable off-axis PSF on source centroids, we restricted the search to sources within 7′ of the telescope boresight. This region contained seven *Tycho-2* sources and 50 *Chandra* sources in the

[9] See § 6.3 of the *Chandra* Proposer's Observatory Guide Rev. 2.0, hereafter the POG, for the definition of the ACIS flight grades and their correspondence with *ASCA* grades.

[10] A description of the "flaring-pixel" or "cosmic-ray afterglow" problem in the ACIS frontside-illuminated CCDs is available from the CXC at http://asc.harvard.edu/ciao/caveats/acis.html.

[11] See the note from the ACIS Instrument Team posted at http://asc.harvard.edu/ciao/caveats/acis_cray.html.

TABLE 1
X-Ray Positions and Count Rates

Number	CXOGC Name	R.A. (J2000.0)	Decl. (J2000.0)	Count Rate[a] (10^{-3} counts s^{-1})	Identification[b]
1	J174525.7−285627	17 45 25.779 ± 0.017	−28 56 27.08 ± 0.14	1.52 ± 0.20	TYC 6840-666-1[c]
2	J174530.0−290704	17 45 30.015 ± 0.015	−29 07 04.22 ± 0.12	11.53 ± 0.55	TYC 6840-020-1[d]
3	J174538.0−290022	17 45 38.058 ± 0.012	−29 00 22.18 ± 0.08	6.36 ± 0.40	...
4	J174539.4−290031	17 45 39.455 ± 0.013	−29 00 31.92 ± 0.11	1.30 ± 0.23	AF NW?[e]
5	J174539.7−290020	17 45 39.785 ± 0.012	−29 00 20.17 ± 0.09	4.89 ± 0.37	...
6	J174539.7−290022	17 45 39.771 ± 0.012	−29 00 22.97 ± 0.09	3.38 ± 0.32	...
7	J174539.7−290029	17 45 39.759 ± 0.012	−29 00 29.85 ± 0.10	2.76 ± 0.30	IRS 13
8	J174540.0−290027	17 45 40.023 ± 0.012	−29 00 27.98 ± 0.08	5.74 ± 0.40	Sgr A*
9	J174540.9−290014	17 45 40.957 ± 0.012	−29 00 14.16 ± 0.09	2.47 ± 0.28	...
10	J174543.9−290456	17 45 43.919 ± 0.012	−29 04 56.49 ± 0.11	3.52 ± 0.30	TYC 6840-590-1

Note.—Units of right ascension are hours, minutes, and seconds; units of declination are degrees, arcminutes, and arcseconds.
[a] Count rate in the 0.5–7.0 keV band.
[b] *Tycho-2* identifiers are from Høg et al. 2000.
[c] Optical identifier: CSI-28-17423 (B star).
[d] Optical identifiers: HD 316224 (F2 star); HIP 86911 (parallax = 10.73 mas).
[e] Tentative identification (§ 6).

0.5–1.5 keV band. We found three matches using a correlation radius of 2″ (see Table 1). The expected number of false matches is 7.9×10^{-3}; this quantity is equivalent to the cumulative probability of getting at least one false match. The probability of getting three matches out of seven trials by random chance is 5.1×10^{-8}. It is therefore highly likely that all three matches are real. The astrometric uncertainties listed in the *Tycho-2* catalog for the positions and proper motions of the three reference stars are in the ranges 25–104 mas and 1.8–4.3 mas yr^{-1}, respectively.

We computed the source offsets (*Tycho-2* position−*Chandra* position) and fitted for a rotation and translation of the field. No significant rotation was found, so we refitted for a translation only. The best-fit parameters were $\Delta\alpha = +0\farcs00 \pm 0\farcs07$ and $\Delta\delta = -0\farcs36 \pm 0\farcs07$ (1 σ). After correcting the aspect solution for the offset in declination, the residual rms scatter in the X-ray positions of the *Tycho-2* sources was 0.″26 in right ascension and 0.″12 in declination; hence the astrometric uncertainty in both directions of the registered field center is 0.″16.

3.3. *Adaptive Smoothing and Flat-fielding of the Images*

We generated a broadband count image of the center of our Galaxy by binning the 0.5–7 keV counts into a two-dimensional image, but it suffered from the effects of the mirror vignetting and the gaps between the CCDs. In addition, it was difficult to see the low surface brightness extended emission. Here we describe a method that we developed for smoothing and flat-fielding the count image to remove these effects.

The mirror vignetting and the effective area curve for the combined HRMA/ACIS instrument are both energy dependent (see Figs. 4.3 and 6.9 of the POG). Therefore, we split the broad band into several narrower bands to minimize variations of the effective area across each band, while at the same time creating images with a reasonable number of counts in astrophysically interesting bands. Based on these criteria, we created narrowband images in the 0.5–1.5, 1.5–3, 3–6, and 6–7 keV bands. We then created monochromatic exposure maps at 1, 2.4, 5, and 6.4 keV; these energies were selected because the effective area at each energy roughly approximated the mean effective area over the corresponding band, after allowing for the characteristically steep spectral shape of Galactic X-ray sources and the large column density toward the Galactic center. The narrowband images and the corresponding exposure maps were then blocked using 6 × 6 pixel (3″ × 3″) bins to increase the chances of getting at least one count per bin within the chip-gap regions and to cut down on the computational time in subsequent steps.

Next we adaptively smoothed the broadband image using minimum and maximum signal-to-noise thresholds of 3 and 5 σ, respectively (Ebeling, White, & Rangarajan 2001). The background level was computed locally. The size of the Gaussian smoothing kernel used at each point in the broadband image was output to a scale map, which was fed back into the smoothing algorithm as we smoothed each narrowband image and exposure map so that all images and maps were adaptively smoothed in exactly the same way. After smoothing, we divided each image by its corresponding exposure map to produce a flat-fielded narrowband image; these narrowband images were then added together to produce a flat-fielded broadband image.

4. X-RAY IMAGES OF THE GALACTIC CENTER

In Figures 2–4, we present an exploded view of the center of our Galaxy made with *Chandra*/ACIS-I in the 0.5–7 keV band. These images have been adaptively smoothed and flat-fielded as described in § 3.3. Remarkable structure in the X-ray emission from the Galactic center is revealed for the first time with sufficient angular resolution to allow detailed comparisons with features seen in the radio and IR bands (see Fig. 1).

Figure 2 is a false-color image with logarithmic scaling of the full 17′ × 17′ ACIS-I field of view, covering the central 40 pc × 40 pc of the Galaxy. The Galactic plane is marked by a white line. Numerous point sources and bright, complex diffuse emission are readily visible. The diffuse X-ray emission is strongest in the vicinity of the Sgr A complex (*red region*). The Sgr A complex sits on a ridge of emission (*green and blue*) extending north and east parallel to the Galactic plane that was first seen by *Einstein* (Watson et al. 1981) and later observed by *ROSAT* (Predehl & Trümper

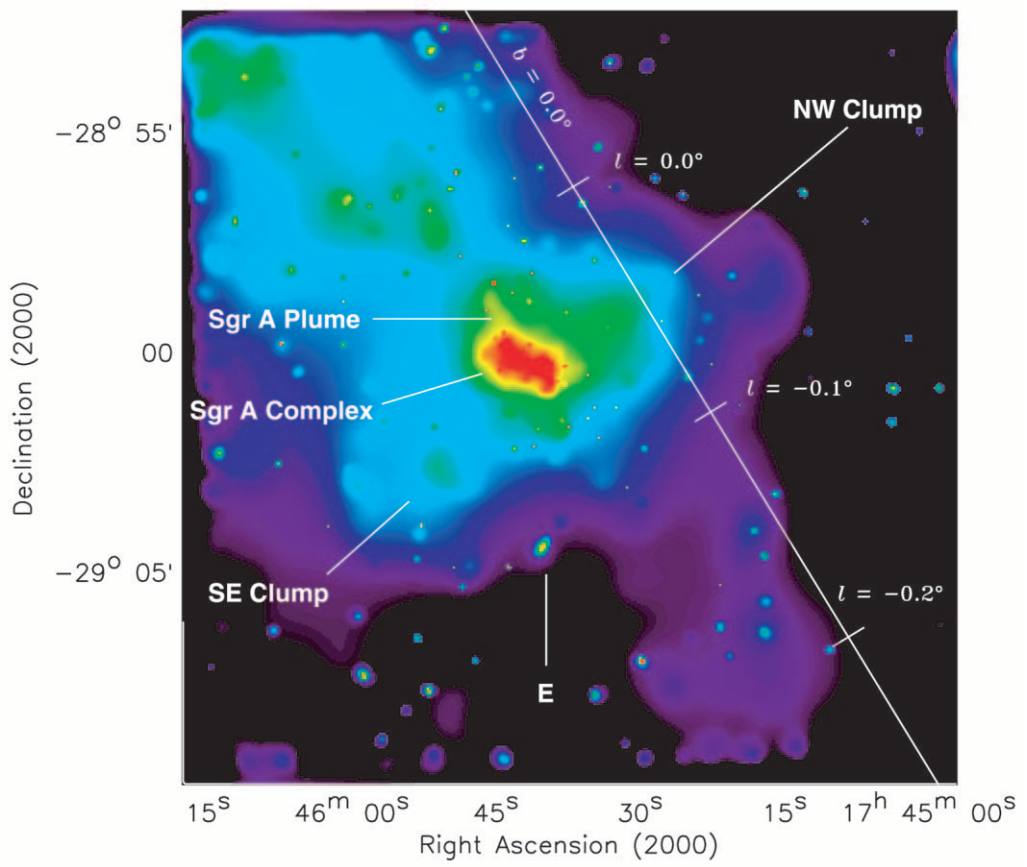

FIG. 2.—0.5–7 keV image with logarithmic scaling of the central 17′ × 17′ of the Galaxy (§ 4). The image has been adaptively smoothed and flat-fielded to bring out the low surface brightness emission and to remove the effects of the mirror vignetting and the gaps between the CCDs. The red region at the center is X-ray emission from the Sgr A complex. This emission fills the center of the nonthermal radio shell source Sgr A East and sits on a ridge of X-ray emission (*green and blue*) extending north and east parallel to the Galactic plane (*white line*).

1994), *ASCA* (Koyama et al. 1996), and *BeppoSAX* (Sidoli et al. 1999b). This ridge is most sharply defined in the 3–6 keV band, with clumps of bright emission visible in the 6–7 keV band. Spectral analysis of the *ASCA* data by Koyama et al. indicated that this emission is from a thermal plasma with $kT \approx 10$ keV, but our preliminary analysis of the *Chandra* data suggests the emission is from a much cooler gas, $kT \approx 3$ keV, once emission from point sources is removed. Wang, Gotthelf, & Lang (2002) report a similar result from a *Chandra*/ACIS-I survey of the central $2^\circ \times 0.^\circ 8$ of the Galaxy.

On the eastern side of the Sgr A complex lies the nonthermal radio shell source Sgr A East, the origin of which has been a topic of debate since its discovery. It has been interpreted by some as a supernova remnant (SNR; Jones 1974; Ekers et al. 1983), but alternative origins have been proposed as well (e.g., Yusef-Zadeh & Morris 1987; Mezger et al. 1989; Kundt 1990; Khokhlov & Melia 1996). Our detailed study of the X-ray counterpart (Maeda et al. 2002) argues strongly that Sgr A East is a rare type of metal-rich, "mixed-morphology" supernova remnant that may have been produced about 10,000 yr ago by the Type II explosion of a 13–20 $M_\odot$ progenitor. The X-ray emission from Sgr A East is concentrated in the central 2–3 pc within the 6 pc × 9 pc radio shell and offset about 2 pc from Sgr A*. The spectrum is produced by an optically thin thermal plasma with $kT \simeq 2$ keV, strongly enhanced metal abundances, and elemental stratification.

A curious linear feature ~0.′5 long (yellow) projects from the northeast toward the center of Sgr A East. It appears as a plume of emission extending north from Sgr A East. The brightest part of the Sgr A Plume is located at R.A. = $17^h45^m44.^s4$, decl. = $-28^\circ59'36''$ (J2000.0). It is clearly present in narrowband count maps in the 1.5–3 and 3–6 keV bands, but it is not visible in the 6–7 keV band. This is in contrast to the core X-ray emission from Sgr A East, which dominates the 6–7 keV band because of its strong Fe-Kα line emission.

Emission (*green and blue*) extending perpendicular to the Galactic plane through the position of Sgr A* on a scale of ~10 pc is clearly visible. This emission lies within the radio structure known as the Sgr A Halo that surrounds Sgr A East, Sgr A West, and Sgr A* in projection. A *BeppoSAX* observation in 1998 with 1′ resolution discovered soft X-ray emission (2–5 keV) that was spatially correlated with the triangular-shaped radio halo (Sidoli & Mereghetti 1999a). Sidoli & Mereghetti fitted the data with an absorbed thin thermal plasma model and obtained a best-fit temperature of ~0.6 keV. They concluded that the soft X-ray emission was consistent with thermal emission from an evolved supernova remnant associated with the Sgr A East shell.

The *Chandra* data, however, reveal a much more complex picture. The emission perpendicular to the Galactic plane is resolved for the first time into bright clumps on either side of the plane along a line passing through the position of Sgr A* and *not* the center of Sgr A East. These clumps are

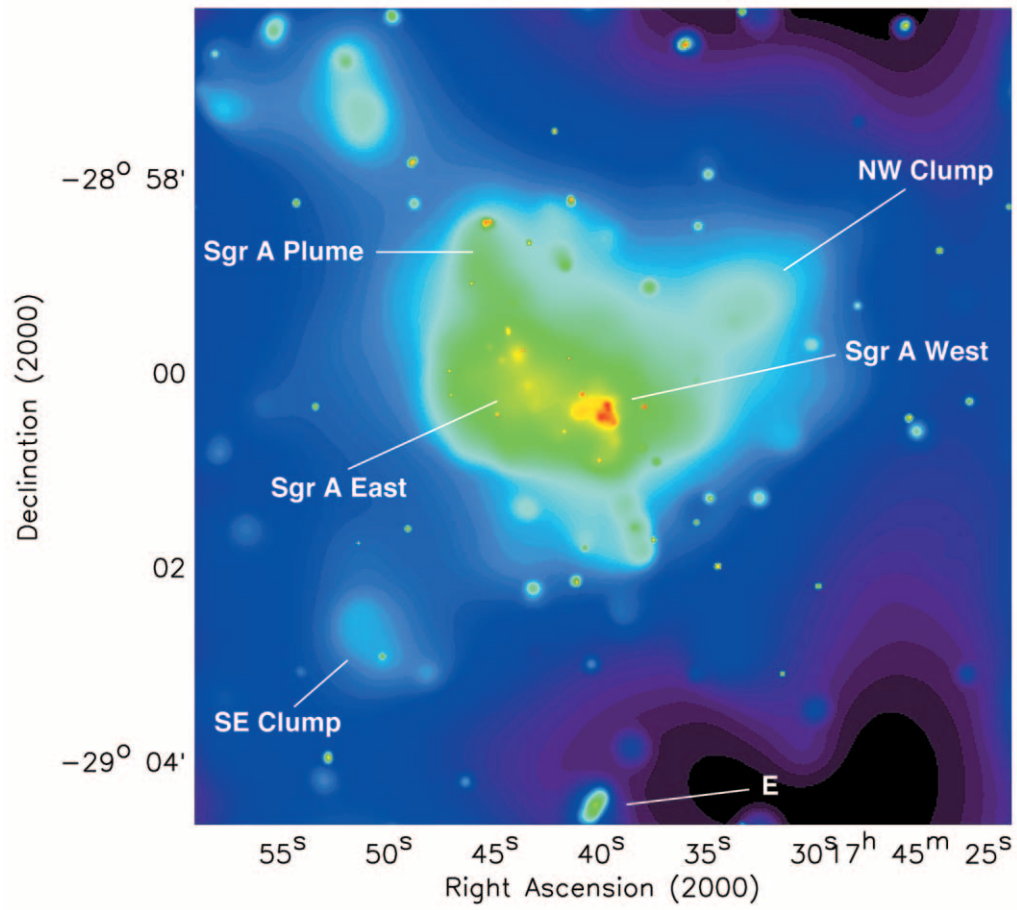

FIG. 3.—0.5–7 keV image with logarithmic scaling of the central 8′.4 × 8′.4 of the Galaxy (§ 4). The intricate structure of the X-ray emission from the vicinity of the Sgr A complex (*yellow and green*) is resolved for the first time. The image has been adaptively smoothed and flat-fielded. X-ray emission from the compact, nonthermal radio source Sgr A* is just discernible as the southeastern component of the red structure at the center of the image.

labeled "NW" and "SE" in Figures 2 and 3. They are not apparent in the *BeppoSAX* image of Sidoli & Mereghetti except as the corners of the triangle representing the halo of Sgr A*. The emission in these clumps is strong in the 1.5–6 keV band but weak at 6–7 keV, in contrast with Sgr A East, which dominates the 6–7 keV map (see Fig. 2 of Maeda et al. 2002). Thus, the spectral and spatial evidence lead us to suggest that the emission oriented perpendicular to the plane along a line passing through the Galactic center may be unrelated to Sgr A East. Instead, these features may indicate the presence of a hot, "bipolar" outflow from the vicinity of the SMBH. In that case, the X-ray–emitting plasma may be escaping preferentially along magnetic field lines, which, at the center of the Galaxy, run perpendicular to the Galactic plane to within about 20° (Morris & Yusef-Zadeh 1985; Anantharamaiah et al. 1991; Morris & Serabyn 1996; Lang, Morris, & Echevarria 1999). The triangular shape of the Sgr A Halo may be the result, therefore, of overlapping structures with disparate origins in the central parsecs of the Galaxy.

The *Chandra* data also revealed for the first time an elongated X-ray structure, CXOGC J174540.3−290429, about 4′ south of Sgr A* that is coincident with the nonthermal radio source denoted Sgr A-E "wisp" by Ho et al. (1985). The position of the X-ray source is marked with an "E" in Figures 2 and 3. Ho et al. suggest that the radio structure may be part of a previously undetected supernova remnant in the Galactic center. The X-ray source is ∼15″ long, or ∼0.6 pc if it is at 8 kpc, and shows a featureless spectrum with strong absorption. Sakano et al. (2003) have interpreted the data from our *Chandra* observation and data from an observation they performed with *XMM-Newton* as a new nonthermal X-ray filament (XMM J174540−2904.5). We will present our analysis of this feature based on the supernova model of Ho et al. (1985) in another paper.

Figure 3 is an expanded view centered on Sgr A* of the inner 8′.4 × 8′.4 of the field. This image was created using the procedure described above, starting with 2 × 2 pixel bins. Complex structures can be seen in the X-ray emission from the vicinity of Sgr A East (*yellow and green*). The Sgr A Plume discussed above in Figure 3 is aligned with a string of clumps or knots (yellow) within Sgr A East, implying that this feature might in fact be physically related to Sgr A East rather than simply a chance superposition on the sky. X-ray emission that we associate with the compact, nonthermal radio source Sgr A* is just discernible as the southeastern component of the red structure at the center of the image. In addition, there is a clump of bright emission (yellow) centered ≈0.3 pc east of Sgr A*.

Figure 4 is a 1′.3 × 1′.5 close-up around Sgr A* (red dot at R.A. = $17^{h}45^{m}40^{s}.0$, decl. = −29°00′28″, J2000.0) overlaid with VLA 6 cm contours of Sgr A* and Sgr A West (F. Yusef-Zadeh 1999, private communication). The image was created as described above, starting with a

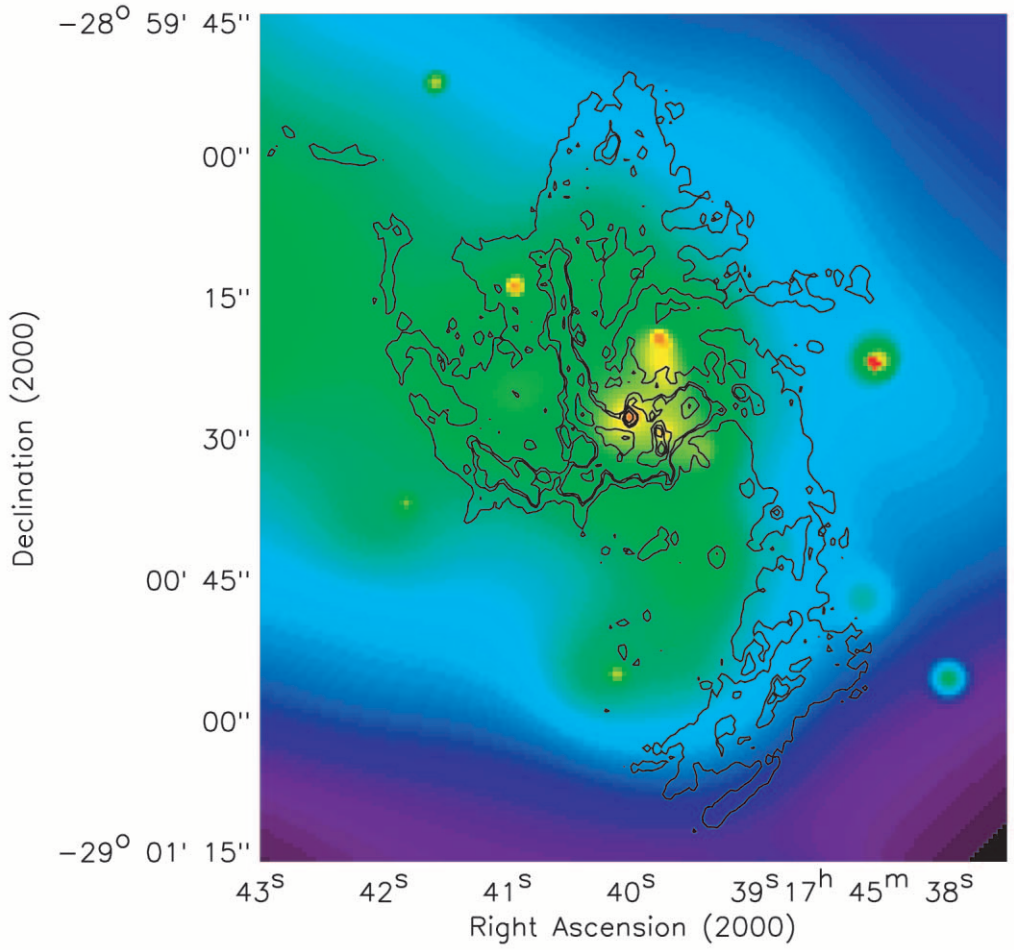

FIG. 4.—0.5–7 keV image with logarithmic scaling of the central 1′.3 × 1′.5 of the Galaxy (§ 4). The image has been adaptively smoothed and flat-fielded. Overlaid on the image are VLA 6 cm contours of Sgr A* and Sgr A West from F. Yusef-Zadeh (1999, private communication). X-ray emission from the vicinity of Sgr A* appears as a red dot at R.A. = $17^h45^m40^s.0$, decl. = −29°00′28″. X-ray emission coincident with IRS 13 (*yellow*) is evident just southwest of Sgr A*.

full-resolution image. Sgr A West is an H II region seen in absorption against the nonthermal emission from Sgr A East; consequently, Sgr A West must lie in front of Sgr A East (Yusef-Zadeh & Morris 1987; Pedlar et al. 1989). The absorption is not total, however, so Sgr A West may lie near the front edge of the Sgr A East shell (Pedlar et al. 1989).

The western boundary of the brightest diffuse X-ray emission (*green*) coincides precisely with the shape of the Western Arc of the thermal radio source Sgr A West. On the eastern side, the emission continues smoothly into the heart of Sgr A East (see Fig. 2, *red region*). In addition, the indentation seen in the X-ray intensity ≈25″ southeast of Sgr A* coincides with a molecular emission peak in the circumnuclear disk (CND; Wright et al. 1987; Marr, Wright, & Backer 1993; Yusef-Zadeh, Melia, & Wardle 2000; Wright et al. 2001). Since the Western Arc is believed to be the ionized inner edge of the CND, the morphological similarities between the X-ray and the radio structures strongly suggest that the brightest X-ray–emitting plasma may be confined by the western side of the CND. This may be evidence that Sgr A West and Sgr A* physically lie within the hot cavity inside the Sgr A East shell; if this is true, and if Sgr A East is a supernova remnant, then Sgr A* may have been brighter a few hundred years ago (Koyama et al. 1996; Murakami et al. 2000, 2001) as the supernova shock wave swept through the position of the SMBH. We discuss this possibility further in our paper on the X-ray emission from Sgr A East (Maeda et al. 2002). The alternative possibility, that Sgr A East and Sgr A West occupy physically separate regions of space, requires a chance alignment of the CND along our line of sight to the western edge of Sgr A East. The morphological similarities would then be simply the result of obscuration by the molecular gas and dust in the CND. In this case, the blast wave would be free to expand past the western edge of the CND (in projection) and would eventually show up as increased surface brightness to the west of the CND. This explanation therefore requires a chance alignment in both space and time.

We are using the narrowband images described above to study the distribution of hard and soft point sources in the field and to study the morphology of the bright Fe Kα line emission first observed by *Ginga* (Koyama et al. 1989). These results will be presented elsewhere.

5. X-RAY EMISSION FROM THE POSITION OF SGR A*

5.1. *Position*

Figure 5 shows a 1′ × 1′ field centered on the position of Sgr A* and made from the counts in the 0.5–7 keV band.

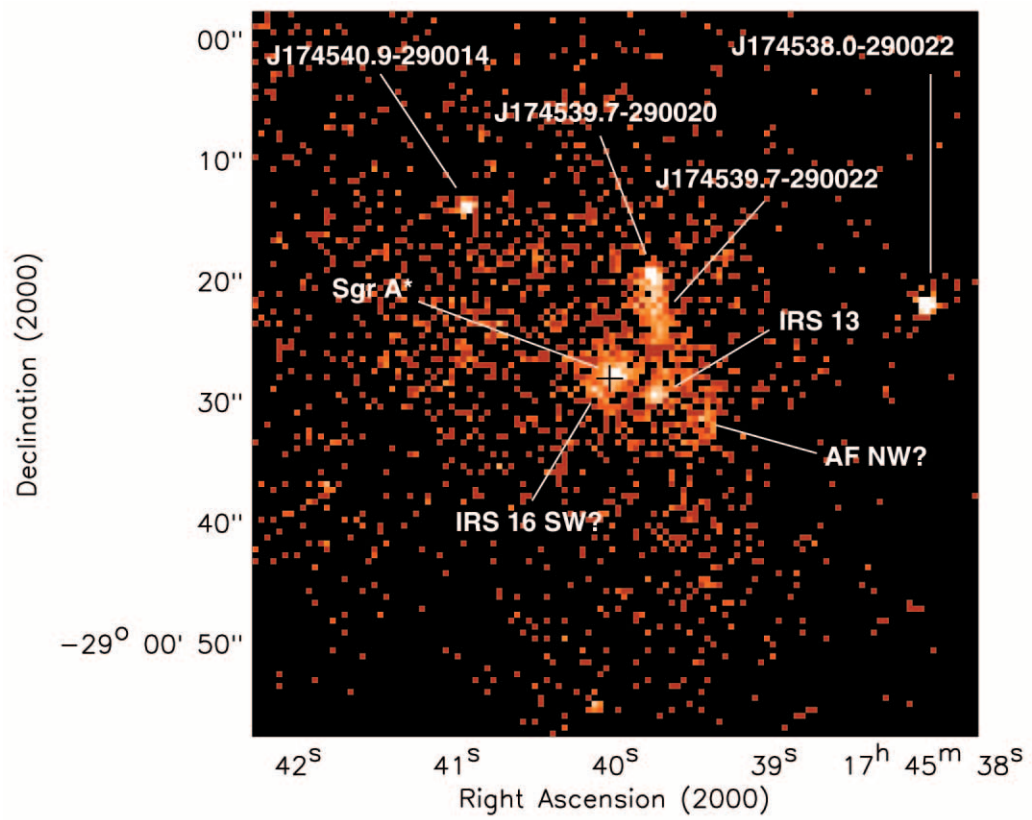

FIG. 5.—0.5–7 keV image with logarithmic scaling of the central $1' \times 1'$ of the Galaxy (§ 5.1). This image has not been smoothed or flat-fielded. Each pixel subtends a solid angle of $0''.492 \times 0''.492$ on the sky. The black cross marks the radio position of Sgr A* (Reid et al. 1999). The cross lies superposed on the X-ray source that we associate with Sgr A* based on the extremely close positional coincidence. A relatively strong X-ray source is associated with the complex of stars in the luminous IR source IRS 13 (§ 6). A weaker X-ray source is coincident within $0''.52$ with the IR source AF NW, but the uncertainty in the X-ray position is $\approx 0''.2$ so the identification is tentative. We have marked the possible detection of an X-ray source that would coincide with IRS 16SW within $\approx 1''$. There appears to be a significant excess of counts at this location, but the wavelet algorithm did not identify a source there, possibly because of its proximity to the brighter source at the position of Sgr A*. The sources labeled with their CXOGC names have no corresponding IR source in Ott et al. (1999). The brighter of these sources are likely candidates for new X-ray binaries. Bright diffuse emission from hot gas and a population of faint point sources are visible throughout the region.

This image has not been smoothed or flat-fielded. The black cross marks the radio interferometric position of Sgr A* as determined by Reid et al. (1999). Clearly visible at the center of the image is the X-ray source, CXOGC J174540.0−290027, that we associate with Sgr A* based on the extremely close positional coincidence. The measured position of CXOGC J174540.0−290027 differs from the radio position of Sgr A* by $0''.27$, corresponding to a maximum projected distance of 12 lt-days (see Table 1). The uncertainty in the position of CXOGC J174540.0−290027 is $0''.18$; this is the combination of the uncertainty reported by the source detection algorithm and the uncertainty in the field registration (§ 3.2). Thus, the positions of CXOGC J174540.0−290027 and Sgr A* are completely consistent.

We estimated the probability of detecting a random source that is highly absorbed, as bright or brighter than CXOGC J174540.0−290027, and coincident with Sgr A* within $0''.27$ as follows. As we reported in § 3.2, we have detected 157 sources in the 0.5–7 keV band and 71 sources in the 0.5–1.5 keV band within the ACIS-I field of view. Selecting only those sources that lay within a radius of $8'$ of Sgr A* left us with 143 sources in the 0.5–7 keV band and 62 sources in the 0.5–1.5 keV band, with 24 matches between the two source lists using a correlation radius of $2''$. After removing the foreground sources, the resultant 0.5–7 keV source list contained 119 absorbed sources within $8'$ of Sgr A*. Of these 119 sources, only CXOGC J174538.0−290022 was brighter than CXOGC J174540.0−290027 during the observation.

To determine the radial distribution of the sources on the sky, we counted up the number of sources in concentric annuli centered on Sgr A*, using $1'$ wide annuli, and fitted the distribution with a power-law model. The best-fit radial surface density profile was given by the equation $\Sigma_X(\theta) = (2.6 \pm 0.6)(\theta/1')^{-1.2\pm0.2}$ sources arcmin^{-2}, where θ is the offset angle from Sgr A* in arcminutes. Integrating the profile from $0''$ to $0''.27$ and multiplying by $2/119$, we found that the probability of detecting a random, absorbed source as bright or brighter than CXOGC J174540.0−290027 and coincident with Sgr A* within $0''.27$ was 4.6×10^{-3}. The radial profile given above, however, overpredicts the density of sources at small radii, because the source detection efficiency of the combined HRMA/ACIS instrument drops off with increasing off-axis angle due to the combined effects of the increasing PSF size and the decreasing effective area. The integration required an extrapolation of over an order of magnitude toward smaller radii, so even a small flattening of the slope would have caused a significant decrease in the predicted number of sources in the central arcsecond. The probability given

above should thus be considered an upper limit to the true probability. We will address these problems in our subsequent paper on the point sources.

5.2. *Morphology*

The emission at the position of Sgr A* appears to be more extended than that of the point sources CXOGC J174538.0−290022 and CXOGC J174540.9−290014 (see Fig. 5). To test this, we computed a background-subtracted radial profile of the surface brightness about each source. The source profiles were extracted in 1 pixel wide annuli out to a radius of 7 pixels. The mean background for each of the point sources was estimated from an annulus with inner and outer radii of 7 and 15 pixels, respectively. The outer radius of the background annulus for Sgr A* was 20 pixels; counts from several X-ray point sources within this region were excluded (see § 6).

The radial profiles are shown in Figure 6. The two comparison sources are both heavily absorbed, indicating that they probably lie near the Galactic center. CXOGC J174538.0−290022 is softer than Sgr A*, while CXOGC J174540.9−290014 is harder, so they bracket the energy dependence of the on-axis PSF. Their profiles have been normalized to match the central peak of the Sgr A* profile.

We fitted a Gaussian model to each profile, but the fits to Sgr A* and CXOGC J174538.0−290022 were rejected with 99.996% and 99.968% confidence, respectively. We

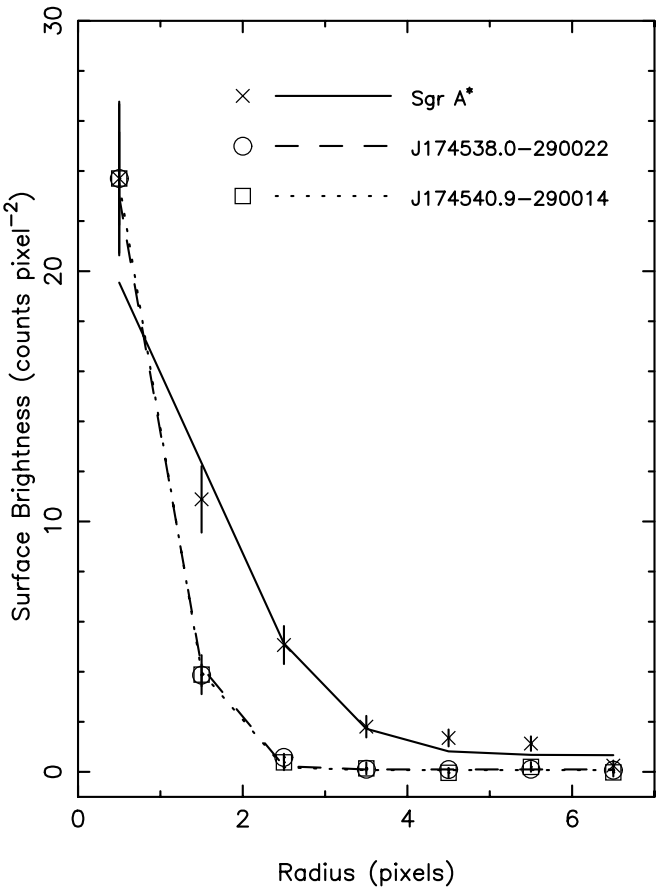

FIG. 6.—Radial profiles of the 0.5–7 keV emission at the positions of Sgr A* and two point sources. The point-source profiles have been normalized to match the central peak of the Sgr A* profile (see § 5.2).

TABLE 2

GAUSSIAN+CONSTANT FITS TO RADIAL PROFILES

Source	Best-Fit Value
Sgr A*:	
Standard deviation (pixels)	1.45 (1.34–1.56)
Normalization (counts pixel^{-2})	20.05 (17.56–22.72)
Constant (counts pixel^{-2})	0.66 (0.50–0.82)
χ^2/dof	12.3/4
J174538.0−290022:	
standard deviation (pixels)	0.76 (0.73–0.80)
Normalization (counts pixel^{-2})	62.64 (56.60–68.75)
Constant (counts pixel^{-2})	0.21 (0.16–0.27)
χ^2/dof	8.0/4
J174540.9−290014:	
standard deviation (pixels)	0.75 (0.70–0.80)
Normalization (counts pixel^{-2})	24.33 (20.72–28.05)
Constant (counts pixel^{-2})	0.06 (0.00–0.13)
χ^2/dof	1.6/4

then added a constant term to each model to allow for an excess in the local background. This yielded acceptable fits to the point sources and a marginally acceptable fit to Sgr A*, for which the probability of exceeding $\chi^2 = 12.3$ with 4 degrees of freedom was 1.5%. The best-fit parameters are presented in Table 2. The curves in Figure 6 show the best-fit models with those of the point sources normalized to the Sgr A* profile. The point-source profiles overlap each other extremely well, while the profile at Sgr A* is nearly twice as broad at greater than 11 σ significance. Additionally, the fit to Sgr A* indicates the presence of an excess local background with a mean surface brightness of 0.66 ± 0.16 counts pixel^{-2}. For comparison, the mean level within the background annulus for Sgr A* was 1.19 ± 0.03 counts pixel^{-2}.

A detailed spatial analysis is beyond the scope of this paper. Here we present a rough estimate of the intrinsic width of the emission at Sgr A* by subtracting in quadrature the mean standard deviation of the point-source profiles from that of the profile at Sgr A*. This yields an estimate of 1.23 ± 0.14 pixels or $0''.61 \pm 0''.07$ for the intrinsic size of the source. Recall that $1''$ corresponds to a projected distance of $\approx$0.04 pc at the Galactic center or $\approx 10^5 R_S$ for a $2.6 \times 10^6\ M_\odot$ black hole.

The origin of the extended X-ray component at Sgr A* is unclear. The scale of the structure is consistent with the expected Bondi accretion radius ($1''$–$2''$; Bondi 1952) for matter accreting hydrodynamically onto the SMBH either from the stellar winds of the nearby cluster of He I/H I emission-line stars (§ 9.1.2) or from the hot diffuse plasma that we observe surrounding Sgr A* (§ 9.3). In some models for Sgr A*, the gas in the accretion flow is thought to be virialized at this distance to a temperature of $\sim 10^7$ K, which is sufficient to emit X-rays in the *Chandra* passband (§ 9.1.1). One possibility, therefore, is that we have detected X-ray emission from gas at the Bondi radius of a hot accretion flow onto Sgr A*. A second possibility is that the extended emission comes from a cusp of stars or stellar remnants. For instance, a neutron-star cluster model has been proposed by Pessah & Melia (2003) to explain the extended emission reported here. The existence of a stellar cusp—as opposed to an isothermal distribution with a flat core—in the central parsec of the Galaxy has been the topic of an ongoing debate (see Alexander 1999 and references therein). A third

possibility is that the extended emission at Sgr A* may be due to colliding-wind emission from the emission-line stars in the central parsec (Krabbe et al. 1995; Blum et al. 1996; Najarro et al. 1997; Paumard et al. 2001). We discuss our search for X-ray emission from these sources in § 6. As noted in that section, counts to the southeast of Sgr A* were excluded from the radial profile to eliminate contamination from the apparent excess near the location of IRS 16SW. This excluded region also covered the positions of IRS 16C and IRS 16CC, which we did not detect in X-rays. The remaining emission-line stars, most of which were not detected in X-rays, appear to lie too far away from Sgr A* to contribute significantly to the extended emission.

5.3. *Spectroscopy*

5.3.1. *Continuum*

A total of 269 counts were extracted in the 0.5–7 keV band from a 1.″5 radius circle centered on the position of the X-ray source coincident with Sgr A*. This aperture was small enough to minimize contamination from several nearby sources described in § 6 and yet large enough that the percentage encircled energy from a point source at the center of the aperture was $\gtrsim 85\%$ at all energies. A local background spectrum with 1144 counts was extracted from a 10″ radius circle centered on Sgr A* (§ 7), excluding counts within a 1.″5 radius of Sgr A* and the other sources in the background region. The net count rate at Sgr A* was $(5.74 \pm 0.40) \times 10^{-3}$ counts s^{-1}.

The source spectrum was grouped to yield 10 counts per bin, resulting in a spectrum with 25 bins. We fitted the spectrum in XSPEC with an absorbed power-law model (see Table 3). The best-fit model (χ^2/dof = 19.8/22) has photon index $\Gamma = 2.7^{+1.3}_{-0.9}$ [$N(E) \propto E^{-\Gamma}$ photons cm^{-2} s^{-1} keV^{-1}] and column density $N_{\rm H} = 9.8^{+4.4}_{-3.0} \times 10^{22}$ cm^{-2}.[12] The source spectrum and the best-fit absorbed power-law model are shown in Figure 7.

[12] Except where specified otherwise, the uncertainties given in this paper are for the 90% confidence interval: $\Delta\chi^2 = 2.71$ for one interesting parameter.

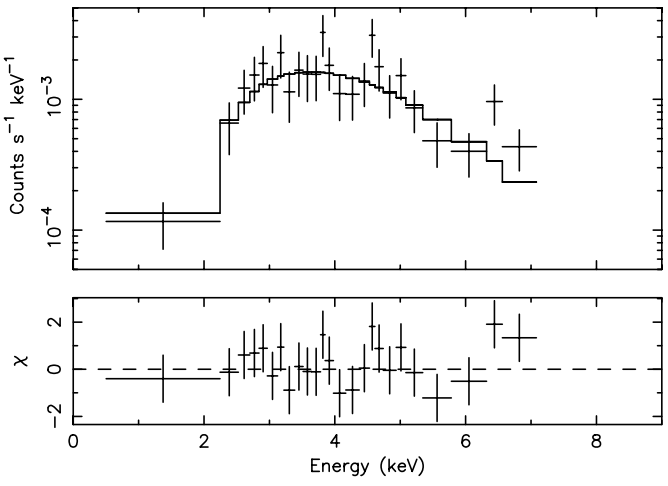

FIG. 7.—Sgr A* spectrum with the best-fit absorbed power-law model (*solid line*; § 5.3.1). Fit residuals are shown in the lower panel. The parameters of the best-fit model are presented in Table 3.

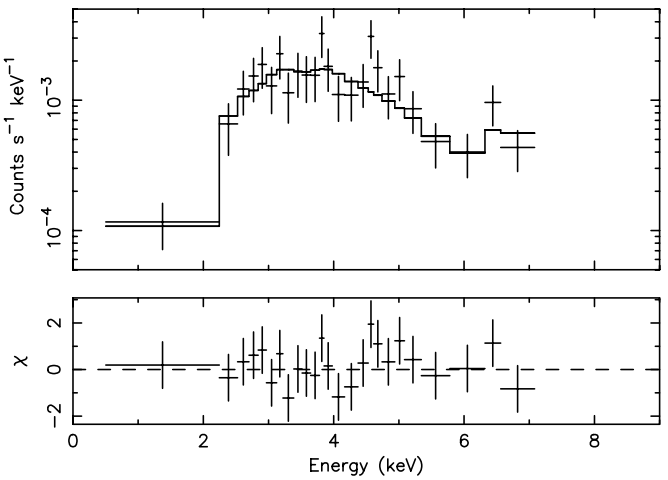

FIG. 8.—Sgr A* spectrum with the best-fit absorbed Raymond-Smith model (*solid line*; § 5.3.1). Fit residuals are shown in the lower panel. The parameters of the best-fit model are presented in Table 3.

We also fitted the source spectrum with an absorbed optically thin thermal plasma model (Raymond & Smith 1977). The best-fit parameters are listed in Table 3. Twice solar abundances were assumed here and throughout the paper (see Morris 1993 and references therein). The best-fit model (χ^2/dof = 16.5/22) has $kT = 1.9^{+0.9}_{-0.5}$ keV and $N_{\rm H} = 11.5^{+4.4}_{-3.1} \times 10^{22}$ cm^{-2}. The source spectrum and the best-fit thermal model are shown in Figure 8.

Both models were consistent with the data because of the low number of counts. Using the power-law model, the observed flux in the 2–10 keV band was $1.3^{+0.4}_{-0.2} \times 10^{-13}$ ergs cm^{-2} s^{-1} and the absorption-corrected luminosity was $2.4^{+3.0}_{-0.6} \times 10^{33}$ ergs s^{-1}. The thermal plasma model gave similar values. Because of the large uncertainties in the photon index and the column density, the 2–10 keV luminosity is known only to within a factor of 2, and the extrapolated 0.5–10 keV luminosity ($\sim 8.5 \times 10^{33}$ ergs s^{-1}) is uncertain by more than an order of magnitude. The confidence limits given for the flux and luminosity of Sgr A* were derived by computing the 90% confidence region ($\Delta\chi^2 = 4.61$ for two interesting parameters) for the column density versus the photon index parameters of the absorbed power-law model with the normalization parameter of the power law free to vary. The column density and photon index were then fixed at the extremum values of the 90% confidence contour, the spectrum was fitted to determine the corresponding best-fit normalization value, and the flux and luminosity of the model were computed.

Next we fitted the absorbed power-law model to the spectrum using a range of fixed column densities: $N_{\rm H} = (6,\ 8,\ 10) \times 10^{22}$ cm^{-2}. As expected, the best-fit photon index became flatter as the column density was decreased. The best-fit photon index was about 1.5 when the column density was fixed at the canonical Galactic center value $N_{\rm H} = 6 \times 10^{22}$ cm^{-2} (χ^2/dof = 24.2/23). However, a column density this low was only marginally consistent with the data at the 99% confidence level.

The measured spectrum suffers from two known systematic effects. First, the percentage encircled energy focussed by the HRMA within the 1.″5 radius extraction circle is energy dependent, varying from $\approx 95\%$ at 1.5 keV to $\approx 85\%$ at 8.6 keV. Second, charge was lost as events were clocked

out of detector I3 as a result of the increased CTI. This caused an energy-dependent decrease in the number of detected events. From measurements made with the external calibration source at -110°C, it is known that $\approx$5% of events at 1.5 keV and $\approx$20% at 5.9 keV were lost. Hence both effects worked together to lower and to steepen the observed spectrum systematically. This may also have increased the best-fit column density by an unknown amount. Using the numbers above, we estimated that the measured luminosity should be increased by $\sim$20% and the photon index should be decreased (i.e., flattened) by $\sim$0.2–0.3. Given the uncertainties in these corrections and the fact that they are negligible compared to the uncertainties in the model parameters because of low photon statistics, these corrections were not applied to the values in Table 3.

5.3.2. Fe Kα *Line*

Excess counts might be present in the 6–7 keV region of the Sgr A* spectrum (see Fig. 7). To constrain the characteristics of possible iron line emission, we fitted the observed spectrum with an absorbed power-law plus Gaussian-line model. We also fitted the spectrum with an absorbed thermal bremsstrahlung plus Gaussian-line model. In each model, the line was assumed to be narrow because of the poor counting statistics and the moderate spectral resolution of the ACIS detectors. Both models fitted the data equally well ($\chi^2/\mathrm{dof} \simeq 14.5/20$). The best-fit parameters are listed in Table 3. The absorbed thermal bremsstrahlung plus Gaussian model is shown in Figure 9. The addition of a line component steepened the photon index in the

TABLE 3

Spectral Fits to X-Ray Sources in the Central 10″ of the Galaxy

Parameter	Sgr A*	Integrated Point Sources[a]	Local Diffuse Emission
Power-Law Model			
$N_{\rm H}$ (10^{22} cm^{-2})	9.8 (6.8–14.2)	13.2 (10.5–19.7)	...
Γ	2.7 (1.8–4.0)	2.5 (1.9–3.7)	...
Normalization (10^{-4} photons cm^{-2} s^{-1} keV^{-1} at 1 keV)	3.5 (0.6–28.8)	8.2 (2.8–75.0)	...
χ^2/dof	19.8/22	56.3/72	...
Optically Thin Thermal Plasma Model[b]			
$N_{\rm H}$ (10^{22} cm^{-2})	11.5 (8.4–15.9)	...	12.8 (11.4–14.2)
kT (keV)	1.9 (1.4–2.8)	...	1.3 (1.2–1.5)
Normalization (10^{-4} cm^{-5})[c]	5.2 (2.7–12.3)	...	62 (43–87)
χ^2/dof	16.5/22	...	119.1/121
Power-Law plus Gaussian Model			
$N_{\rm H}$ (10^{22} cm^{-2})	11.6 (8.3–17.6)	...	...
Γ	3.5 (2.4–5.3)	...	...
Normalization (10^{-4} photons cm^{-2} s^{-1} keV^{-1} at 1 keV)	11.5 (1.7–21.7)	...	...
Line energy (keV)	6.5 (6.4–7.0)	...	...
Sigma (keV)	0.0 (fixed)	...	...
I (10^{-7} photons cm^{-2} s^{-1})[d]	23.2 (8.2–41.6)	...	...
χ^2/dof	14.6/20	...	...
Thermal Bremsstrahlung plus Gaussian Model			
$N_{\rm H}$ (10^{22} cm^{-2})	10.0 (7.3–14.0)	...	10.1 (9.4–11.8)
kT (keV)	2.2 (1.3–4.2)	...	1.6 (1.3–2.0)
Normalization (10^{-4} cm^{-5})[f]	2.8 (0.9–11.6)	...	24.0 (14.8–48.4)
Line Energy (keV)	6.5 (6.4–6.9)	...	6.5 (6.3–6.6)
Sigma (keV)	0.0 (fixed)	...	0.0 (fixed)
I (10^{-7} photons cm^{-2} s^{-1})[e]	23.9 (9.8–41.0)	...	56.2 (28.3–82.2)
χ^2/dof	14.4/20	...	119.3/119
Flux and Luminosity (2–10 keV)[f]			
$F_{\rm X}$ (10^{-13} ergs cm^{-2} s^{-1})	1.3 (1.1–1.7)	4.0 (3.3–4.5)	6.0 (5.6–6.2)[g]
$L_{\rm X}$ (10^{33} ergs s^{-1})	2.4 (1.8–5.4)	7.8 (6.0–19.4)	24 (18–32)[g]

Note.—Uncertainties on the model parameters are 90% confidence intervals computed using $\Delta\chi^2 = 2.71$ for one interesting parameter. Uncertainties on the fluxes and luminosities are 90% confidence intervals computed using $\Delta\chi^2 = 4.61$ for two interesting parameters (§ 5.3.1). See § 5.3.1, § 6, and § 7 for details.

[a] Counts within 1″ Sgr A* were excluded from the integrated spectrum of the point sources within the central 10″ of the Galaxy.

[b] Raymond & Smith (1977) model with twice solar elemental abundances.

[c] Normalization $= 10^{-14} \int n_e n_i dV/4\pi D^2$, where n_e and n_i are the electron and ion densities (cm^{-3}) and D is the distance to the source (cm).

[d] Normalization $= 3.02 \times 10^{-15} \int n_e n_i dV/4\pi D^2$, where n_e and n_i are the electron and ion densities (cm^{-3}) and D is the distance to the source (cm).

[e] Line flux.

[f] $F_{\rm X}$ is the observed flux, uncorrected for absorption. $L_{\rm X}$ is the absorption-corrected luminosity. The flux and luminosity of Sgr A* were derived using the best-fit parameters of the power-law model; the optically thin thermal plasma model gave similar values.

[g] Divide by $\pi \times 10^2$ arcsec^2 to convert to surface brightness.

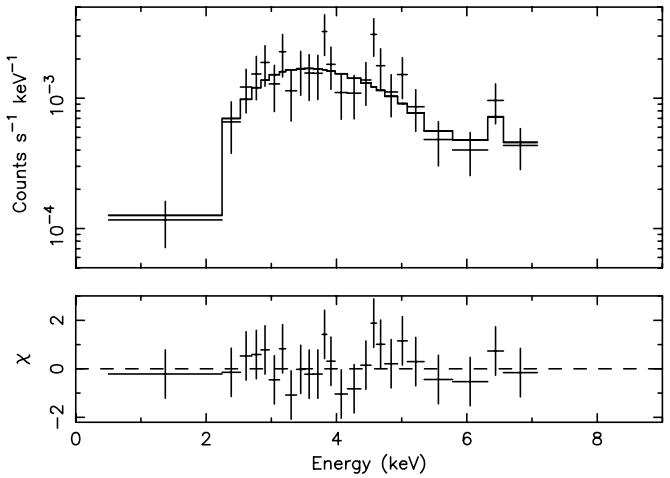

FIG. 9.—Sgr A* spectrum with the best-fit absorbed thermal bremsstrahlung plus Gaussian model (*solid line*; § 5.3.2). Fit residuals are shown in the lower panel. The parameters of the best-fit model are presented in Table 3.

power-law model from 2.7 to 3.5, while the temperature in the thermal model increased from 1.9 to 2.2 keV. The column density changed by less than 20%. The estimated line energy, $6.5^{+0.4}_{-0.1}$ keV, was consistent with either neutral or helium-like Fe Kα. The equivalent width of the line was 1.6 keV in the power-law model and 2.2 keV in the thermal model. Acceptable fits without a line component were obtained in the previous section, so these equivalent widths must be treated as upper limits.

For comparison, the equivalent width of iron in the spectrum of the local diffuse emission within 10″ of Sgr A* was 1.3 keV (§ 7). We assumed in our analysis that the background was spatially uniform. In that case, the background would have contributed only 13% of the counts in the aperture used to extract the Sgr A* spectrum. Furthermore, the background-subtracted spectrum of the integrated emission from the point sources within 10″ of Sgr A* showed no sign of excess counts in the 6–7 keV range (§ 6). If the background is strongly peaked at Sgr A* (§ 5.2), however, then it is possible that the apparent excess in the Sgr A* spectrum may have resulted from an inadequate subtraction of the iron line from the local diffuse background. Thus, poor statistics prevent definitive conclusions on the presence of an iron emission line (or line complex) in the Sgr A* spectrum with these data.

5.4. *Variability*

5.4.1. *Short Timescale*

To examine the short-timescale temporal behavior of the emission at Sgr A*, we constructed a light curve of the net 2–7 keV events within 1.″5 of the source, using the background region described in § 5.3.1. We excluded the final 1.8 ks of the observation to eliminate any residual contamination from the solar activity described in § 3.1. The remaining exposure time was 39.1 ks, and the mean rate was $(5.33 \pm 0.37) \times 10^{-3}$ counts s^{-1}. The light curve is displayed in Figure 10.

The first 3–4 ks of the observation appears to show excess counts. Because of the low count rate and the short duration of the feature, we could not apply a χ^2 test to the binned light curve. Instead, we tested the null hypothesis that the

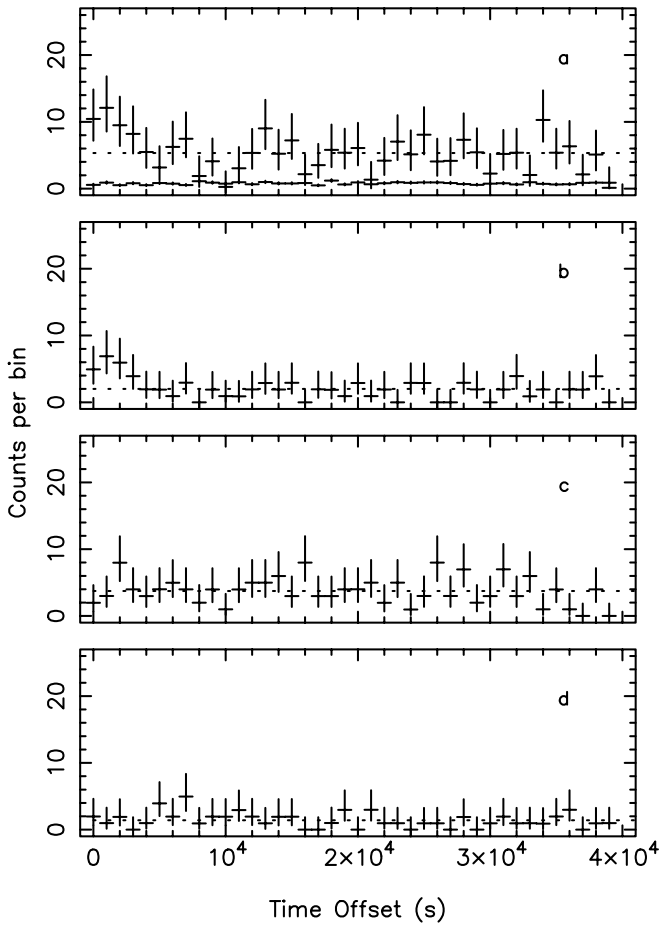

FIG. 10.—Light curves of Sgr A* and two nearby point sources in the 2–7 keV band: (*a*) net events within 1.″5 of Sgr A*, (*b*) net events within 0.″5 of Sgr A*, (*c*) net events within 0.″5 of CXOGC J174538.0−290022, and (*d*) net events within 0.″5 of CXOGC J174540.9−290014. Data points are plotted with two-sided errors (1 σ; Gehrels 1986). Mean count rates are indicated by dotted lines. The bin size is 1 ks. The background rate within 1.″5 of Sgr A* is indicated by the data points near the bottom of (*a*). Both Sgr A* light curves seem to show excess counts during the first 3–4 ks of the observation. The other light curves do not exhibit similar excesses during this interval (see § 5.4.1 for details).

source was constant by performing a Kolmogorov-Smirnov (K-S) test on the arrival times of all events within the source region. The results are presented in Table 4. The probability of exceeding the observed K-S statistic, $P(>\text{K-S}) = 6.7\%$, indicated that the distribution of photon arrival times was consistent with a constant rate. The emission at Sgr A* was extended, however, with a light-crossing time of order a month (§ 5.2), which would dilute variability from a compact region around the SMBH. Consequently, we repeated the analysis on events within 0.″5 of Sgr A*. This yielded a goodness-of-fit probability of 0.66%, indicating that the hypothesis of constancy could be rejected with 99.34% confidence. As a check, we applied the K-S test to all events within 0.″5 of CXOGC J174538.0−290022 and CXOGC J174540.9−290014. In each case, the distribution of arrival times was consistent with no variability (see Table 4). The net count rates within 0.″5 of Sgr A*, CXOGC J174538.0−290022, and CXOGC J174540.9−290014 were $(2.01 \pm 0.22) \times 10^{-3}$, $(3.74 \pm 0.31) \times 10^{-3}$, and $(1.41 \pm 0.19) \times 10^{-3}$ counts s^{-1}, respectively. Thus, Sgr A* was 16

TABLE 4
KOLMOGOROV-SMIRNOV TEST FOR VARIABILITY

Source	Radius of Aperture	Number of Events	K-S Statistic	$P(>\text{K-S})$[a]
Sgr A*.....	1.″5	244	0.0827	0.0671
Sgr A*.....	0.″5	83	0.183	0.00655
J174538.0−290022.....	0.″5	150	0.0594	0.652
J174540.9−290014.....	0.″5	58	0.157	0.102

[a] A low probability indicates that the data are poorly fit by a constant photon-rate model.

times more likely to have varied than CXOGC J174540.9−290014, even though it was 43% brighter.

The K-S test is known to be less sensitive when the maximum absolute deviation from the assumed cumulative distribution function occurs near the ends of the distribution. The apparent flare occurred at the beginning of our observation, and hence the true confidence level for variability should be even higher than stated above. We conclude that a compact component within the source at Sgr A* flared by up to a factor of 3 over a period of 3–4 ks at the start of the observation. The peak 2–10 keV luminosity of the flare was $\simeq 7 \times 10^{33}$ ergs s^{-1}.

Additional data are needed to characterize the duty cycle and luminosity function of X-ray flares from Sgr A*. The study of rapid X-ray variability is of crucial importance, since it has the potential to provide a powerful discriminator between SMBH and stellar origins for the X-ray source and between the various proposed accretion and emission models for Sgr A*.

5.4.2. *Long Timescale*

Observations of the Galactic center with previous X-ray missions suggested the presence of a long-term variable source near the position of Sgr A* (§ 2.2). These observations were made mainly in the hard X-ray band with moderate resolution ($\gtrsim 1'$) instruments. Thus other (transient) sources may have contributed to the measured fluxes. In the following sections, we model the pointlike (§ 6) and diffuse (§ 7) emission observed with *Chandra* in the central 10″ of the Galaxy. Our data show that on 1999 September 21, Sgr A* contributed only 12% of the 2–10 keV flux within this region. All of this emission would have been unresolved by the *ROSAT*/PSPC, which had a spatial resolution of 10″–20″ (FWHM), and most of it would fall within the *XMM-Newton* beam (6″ [FWHM], 15″ [HPD]). Here we use those spectral models to predict *ROSAT*/PSPC count rates and set an upper limit on the luminosity of Sgr A* during the *ROSAT* observation in 1992 March.

Adopting an absorption column of 1×10^{23} cm^{-2}, we refitted the spectra of the three emission components listed in Table 3 and used the best-fit models with the response matrix *pspcb_gain2_256.rsp* to predict the PSPC count rate for each component in the 0.8–2.5 keV band. To convert the surface brightness of the local diffuse emission into an expected count rate, we assumed the counts were extracted from a circular region of radius 20″; for comparison, the 50% encircled energy radius of the PSPC was about 15″–20″. The predicted PSPC count rates were 2×10^{-5} counts s^{-1} for Sgr A*, 3×10^{-5} counts s^{-1} for the integrated point sources, and 6.9×10^{-4} counts s^{-1} for the local diffuse emission. Summing these contributions, the predicted PSPC count rate in 1999 September would have been 7.4×10^{-4} counts s^{-1}. The observed PSPC count rate was $(8 \pm 1) \times 10^{-4}$ counts s^{-1} (Predehl & Trümper 1994), consistent with the ACIS-based prediction.

Assuming that the total flux of the point sources and the local diffuse emission was the same at each epoch, we estimate that the 3 σ upper limit on the PSPC count rate of Sgr A* in 1992 March was 4.6×10^{-4} counts s^{-1}. Taking into account the uncertainty in the luminosity of Sgr A* measured with *Chandra*, the corresponding upper limit on the 2–10 keV luminosity of Sgr A* would have been in the range $(0.4\text{–}1.2) \times 10^{35}$ ergs s^{-1}.

6. STELLAR SOURCES IN THE CENTRAL PARSEC

Four X-ray sources were detected within 10″ of Sgr A*, excluding CXOGC J174540.0−290027. The positions and count rates of these sources are listed in Table 1. CXOGC J174539.7−290029 lies in the midst of IRS 13, which is seen in radio and mid-IR images to be a complex of stars and a diffuse source due to a strong shock at the edge of the "minicavity" (Krabbe et al. 1995; Blum et al. 1996; Najarro et al. 1997; Yusef-Zadeh et al. 2000). Using the IR positions of Ott, Eckart, & Genzel (1999), the position of the X-ray source was determined to be 0.″56 northeast of IRS 13W and 0.″57 southwest of the IRS 13E complex: IRS 13E1, IRS 13E2, and IRS 13E3. Paumard et al. (2001) have taken a high-resolution spectrum at 2.06 μm and argue that IRS 13E3 is a He I emission-line star with a broad P Cygni line profile. They propose that IRS 13E3 is one of a group of stars in the central-parsec cluster that are in the Wolf-Rayet (W-R) stage. Coker, Pittard, & Kastner (2002) have modeled our data for this source as X-ray emission from colliding winds of a W-R binary in which the primary has evolved past the luminous blue variable (LBV) phase.

The apparently diffuse emission located about 7″ northwest of Sgr A* (see Fig. 5) does not correspond with any excess of radio emission in a VLA 6 cm map of the region made by F. Yusef-Zadeh (1999, private communication; see Fig. 4); on the contrary, there seems to be an absence of radio emission at this location in the radio map. The same is true in the mid-IR (M. Morris, in preparation). Two X-ray sources were detected within this region: CXOGC J174539.7−290020 and CXOGC J174539.7−290022. Neither source matched an IR source within 1″. CXOGC J174539.7−290020 stands out in Figure 4 as the red dot at the northern end of a yellow structure. This structure appears to extend a few arcseconds south of CXOGC J174539.7−290022. To prevent contamination of the background spectrum for Sgr A* (§ 5.3.1), we excluded counts within a 1.″5 radius centered at R.A. = $17^{\rm h}45^{\rm m}39^{\rm s}.7$, decl. = −29°00′26″ (J2000.0).

CXOGC J174539.4−290031 is coincident within 0.″52 with AF NW, which Paumard et al. have shown to be a broad-line He I star. The uncertainty in the X-ray position is about 0.″2, however, so the identification is tentative. More data will be required to determine if this identification is correct.

Figure 5 appears to show excess counts just to the southeast of Sgr A*, in the vicinity of IRS 16SW, although no source was found there by the detection algorithm, perhaps because of its faintness and proximity to the brighter X-ray source located at the position of Sgr A*. Ott et al. (1999) report that IRS 16SW is an eclipsing He-star binary, raising the possibility that we may be seeing X-rays from their colliding stellar winds. Emission at levels of order 10^{32}–10^{33} ergs s^{-1} in the 2–10 keV band is well established in W-R stars (e.g., HD 193793: Koyama et al. 1990, 1994; V444 Cyg, Maeda et al. 1999), where the hard component is attributed to colliding winds in a close binary system. To prevent contamination of the Sgr A* profile (§ 5.2) and spectrum (§ 5.3.1), we excluded counts within a 1.″5 radius centered at R.A. = $17^h45^m40^s.2$, decl. = −29°00′29″ (J2000.0).

We did not detect other members of the IRS 16 cluster, which is known to contain a number of He I stars. Paumard et al. find that IRS 16NE, IRS 16C, IRS 16SW, and IRS 16NW are He stars with narrow P Cygni line profiles and propose that they are in or near the LBV phase. Such stars have substantially weaker hard X-ray emission than colliding-wind W-R binaries.

The stellar identifications presented here were based solely on positional coincidence. Interestingly, no matching IR source was found within 3″ of CXOGC J174538.0−290022, despite the fact that it is the second brightest X-ray source in the entire field and the brightest absorbed source. Likewise, no match was found within 3″ of CXOGC J174540.9−290014. These two sources are therefore likely X-ray binary candidates.

Figure 11 shows the spectrum of the integrated X-ray emission from the four stellar sources detected within 10″ of Sgr A* and the two regions with excess counts described above. The spectrum was fitted with an absorbed power-law model. The best-fit model (χ^2/dof = 56.3/72) is listed in Table 3, along with the integrated flux and luminosity. The net count rate from all of these sources was $(1.4 \pm 0.1) \times 10^{-2}$ counts s^{-1} (0.5–7 keV). The spectrum showed no obvious signs of emission lines. To quantify this statement, we fitted the spectrum with an absorbed Raymond-Smith model. The best-fit column density was implausibly high, $N_H = 24.1^{+5.0}_{-4.4} \times 10^{22}$ cm^{-2}, when the elemental abundances were fixed at twice solar abundances (χ^2/dof = 70.9/72). The column density was reasonable, $N_H = (12.3^{+4.4}_{-2.7}) \times 10^{22}$ cm^{-2}, when the metallicity was allowed to vary, but the abundances were set to zero by the fitting engine (χ^2/dof = 56.4/71).

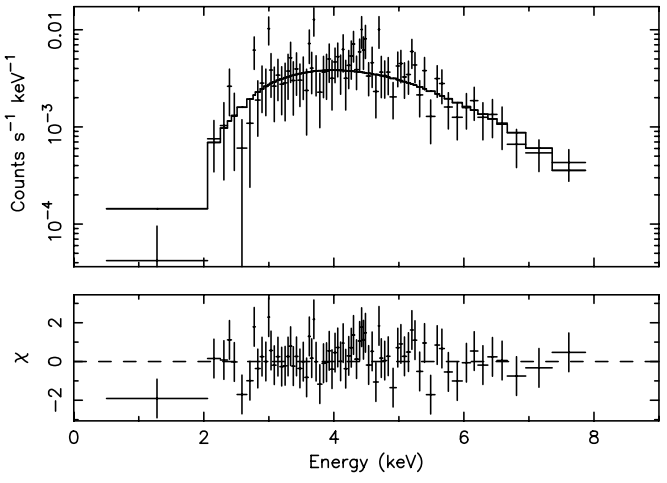

FIG. 11.—X-ray spectrum of the integrated emission from point sources within a 10″ radius of Sgr A* (§ 6). The solid line in the upper panel is the best-fit absorbed power-law model. Fit residuals are shown in the lower panel. The parameters of the best-fit model are presented in Table 3. Note the absence of any feature from Fe line emission in the 6–7 keV range.

7. DIFFUSE EMISSION IN THE CENTRAL PARSEC

The Sgr A complex sits on a ridge of X-ray emission extending parallel to the Galactic plane (§ 4). To study the spectrum of the diffuse emission within 10″ of Sgr A* (hereafter the local diffuse emission), it was necessary to subtract off this underlying background. We selected a region about 42″ north of Sgr A* that lay outside the intense X-ray emission from the Sgr A complex and yet within the extended radio structure known as the Sgr A "halo," where the X-ray surface brightness was relatively flat. We extracted a background spectrum with 544 total counts from a circular region 15″ in radius centered at R.A. = $17^h45^m39^s.7$, decl. = −28°59′47″ (J2000.0). This extraction circle lay entirely on the I3 detector, as did the source extraction circle for the local diffuse emission. The total 0.5–7 keV count rate from this region of the Galactic plane was $(1.9 \pm 0.1) \times 10^{-5}$ counts s^{-1} $arcsec^{-2}$, which was about 24 times higher than the non–X-ray background rate measured in *Chandra*/ACIS observations of high Galactic-latitude fields (see POG § 6.10).

We extracted the source spectrum of the local diffuse emission from a circular region of radius 10″ centered on Sgr A*, excluding emission within 1.″5 of the point sources and regions of excess emission described in § 6. The mean surface brightness of the local diffuse emission was $(1.2 \pm 0.1) \times 10^{-4}$ counts s^{-1} $arcsec^{-2}$ (0.5–7 keV). The background-subtracted spectrum is shown in Figure 12. A strong continuum with line emission from iron (6–7 keV) is clearly visible, and perhaps helium-like sulfur (2.45 keV) and argon (3.14 keV), indicating that most of the emission comes from a hot, optically thin thermal plasma. We fitted the spectrum with an absorbed Raymond-Smith model. The best-fit model (χ^2/dof = 119.1/121) indicated a temperature $kT = 1.3^{+0.2}_{-0.1}$ keV (see Table 3). The 2–10 keV flux and luminosity of the local diffuse emission were $(1.9 \pm 0.1) \times 10^{-15}$ ergs cm^{-2} s^{-1} $arcsec^{-2}$ and $7.6^{+2.6}_{-1.9} \times 10^{31}$ ergs s^{-1} $arcsec^{-2}$.

To measure the energy and equivalent width of the iron emission, we fitted the spectrum with an absorbed thermal bremsstrahlung plus a narrow Gaussian model. The best-fit line energy was $6.5^{+0.1}_{-0.2}$ keV, and the equivalent width was 1.3 keV. The 90% confidence interval on the line energy is inconsistent with He-like iron. While the fit energy is nominally consistent with X-ray fluorescence of cold iron, this would not explain the strong continuum emission. Instead, the best-fit line energy—intermediate between cold and He-like iron—may be evidence that the plasma is in a state of nonionization equilibrium (NIE).

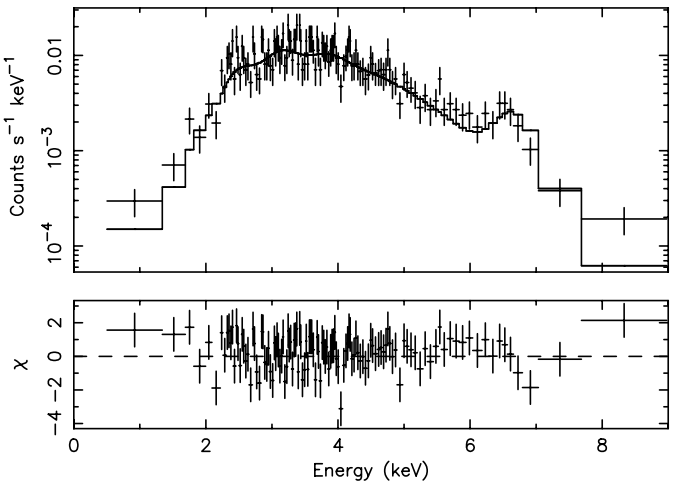

FIG. 12.—X-ray spectrum of the local diffuse background emission within a 10″ radius of Sgr A* (§ 7). The solid line in the upper panel is the best-fit absorbed Raymond-Smith model. Fit residuals are shown in the lower panel. The parameters of the best-fit model are presented in Table 3. Note the presence of strong Fe-line emission in the 6–7 keV range.

Based on the parameters of the best-fit absorbed Raymond-Smith model, we estimate that the local, hot diffuse plasma has an rms electron density $\langle n_e^2 \rangle^{1/2} \approx 26\eta_f^{-1/2}$ cm^{-3} and emission measure EM $\approx 540\eta_f^{-1}$ cm^{-6} pc, where η_f is a filling factor. Here we assumed the plasma is fully ionized with twice solar abundances (mean atomic weight $\mu = 0.70$). The total mass of this gas is $M_{\rm local} \approx 0.1\eta_f^{1/2}\, M_\odot$.

The local plasma around Sgr A* appears to be somewhat cooler than the plasma we analyzed in our study of Sgr A East (Maeda et al. 2002). Using the MEKA thermal plasma model (Mewe, Gronenschild, & van den Oord 1985; Kaastra 1992), Maeda et al. found the Sgr A East plasma has $kT = 2.1^{+0.3}_{-0.2}$ keV. The column densities derived from the fits to both plasmas were consistent at $\sim 1.2 \times 10^{23}$ cm^{-2}. We allowed the elemental abundances to vary when we fitted the high signal-to-noise spectrum of Sgr A East. The best-fit model indicates that the Sgr A East plasma has about 4 times solar abundances. Fitting the local emission near Sgr A* with the abundances fixed at 4 times the solar value did not significantly change the best-fit temperature; hence the difference in temperature between the two plasmas appears to be real.

In addition, Maeda et al. found that the net count rate within a 40″ radius circle centered on Sgr A East at the position R.A. $= 17^{\rm h}45^{\rm m}44\overset{\rm s}{.}1$, decl. $= -29°00'23''$ (J2000.0) was $\approx 3.6 \times 10^{-5}$ counts s^{-1} arcsec^{-2}. Thus, the net count rate from the local diffuse emission was 3.3 times the net count rate within Sgr A East and 6.3 times the total count rate in the background region along the Galactic plane. This shows that the diffuse X-ray emission from the Sgr A complex is significantly peaked in the central parsec of the Galaxy.

Some of the local diffuse emission may be contributed by stars in the central-parsec cluster. Genzel et al. (1996) estimate that the core radius of the cluster is $\sim$0.4 pc (10″) with a stellar-mass density in the core of $\sim 4 \times 10^6\ M_\odot$ pc^{-3}. The 2–10 keV luminosity of 2.4×10^{34} ergs s^{-1} could then arise from the ordinary OB and W-R stars present in the cluster. This level of emission is an order of magnitude higher than seen in young stellar clusters like the Orion Trapezium or W3, but it is comparable to that seen from the R136a cluster and associated W-R stars in 30 Doradus (Feigelson 2001). On the other hand, Alexander (1999) argues that stars in the central 10″ of the Galaxy are distributed in a cusp rather than a flat core. If correct, this could increase the contribution from colliding winds of OB stars.

8. ORIGIN OF THE X-RAY EMISSION AT SGR A*: SMBH OR STELLAR?

Sgr A* is embedded in a cluster of luminous young stars. Sixteen early-type, He I/H I emission-line stars with strong winds (200–1000 km s^{-1}) have been spectroscopically identified within the central $\approx$10″ of our galaxy (Krabbe et al. 1995; Najarro et al. 1997; Paumard et al. 2001). Such stars are thought to be close cousins to stars in the LBV phase and the W-R stage, although their nature is not completely determined. As W-R stars are significant X-ray emitters, especially those in close binaries with other W-R or O stars, one must consider whether the emission we see at Sgr A* arises from accretion onto a SMBH or stellar processes. Ozernoy et al. (1997), for instance, predict that variations with $L_{\rm X} \sim 10^{33}$–10^{35} ergs s^{-1} and durations of order 1 week should occur in the Galactic center cluster as a result of colliding stellar winds.

We recall the X-ray properties described in § 5. First, the position of CXOGC J174540.0−290027 is consistent with the radio position of Sgr A* at the 1.5 σ level, where the 1 σ positional uncertainty is 0.″18. Second, the emission at Sgr A* is resolved with an intrinsic size of $\approx$0.″6 (FWHM). In contrast, the central stellar cluster is a composite structure with a dense compact component 5″ in diameter lying within a larger 20″ diameter component (Eckart, Ott, & Genzel 1999; Paumard et al. 2001), and the compact component (the IRS 16 complex) is centered 2″ east of Sgr A*.

The emission-line stars nearest (in projection) to Sgr A* are IRS 16C, IRS 16NW, and IRS 16SW. As noted in § 6, an excess of counts appears around the position of IRS 16SW, but no X-ray sources are visible in the current data at the positions of IRS 16C and IRS 16NW. Importantly, no bright He I star lies closer than 1.″2 to Sgr A* (Krabbe et al. 1995; Paumard et al. 2001), providing strong evidence against an LBV or W-R origin. Furthermore, the X-ray spectra of single OB and W-R stars are typically quite soft, $kT < 1$ keV, and consequently cannot penetrate the obscuration to the Galactic center.

Close binary W-R+W-R and W-R+O systems with colliding winds can show harder spectra with $kT \simeq$ 1–3 keV and $L_{\rm X} \simeq 10^{32}$–10^{33} ergs s^{-1} in the 2–10 keV band (e.g., Corcoran 1996; Maeda et al. 1999). The spectral and luminosity characteristics of the more extreme W-R binaries are roughly consistent with those of the source coincident with Sgr A*, but the variability reported in § 5.4.1 is inconsistent with the behavior of W-R binaries. Variations associated with binary phase are typically seen on timescales of days to years (e.g., Williams et al. 1990). Variations on timescales of $\sim$1 hr with amplitudes $L_{\rm X} \approx 10^{33}$ ergs s^{-1}, as seen at the position of Sgr A*, are unprecedented among colliding-wind binaries. The detection of rapid variability argues against a binary W-R origin.

To produce the X-ray luminosity via the colliding winds of nonbinaries requires the stars be much closer to each other (a few times 10^{14} cm) than the typical separation of the He I stars in the central parsec (a few times 10^{17} cm). Ozernoy, Genzel, & Usov propose that a

sizeable population of OB stars may be present in the cluster and that X-rays may arise in shocks produced at the interfaces of the winds of these OB stars and the W-R–type emission-line stars. The number of O stars required to obtain a substantial probability for a sufficiently close encounter is $\gtrsim 10^6$, which is far larger than the luminosity constraints allow, so one must again appeal to WR+OB binary systems for anything but an occasional X-ray flare of several weeks duration.

The central few hundredths of a parsec ($\approx 0\farcs5$) surrounding Sgr A* contains a concentration or cusp of at least a dozen bright stars ($K \simeq 14$–16 mag) that are predominantly blue and featureless, indicating that they may be O stars (Eckart et al. 1999). This "Sgr A* (IR)" cluster warrants consideration as the X-ray source, if the winds from these stars are typical of O stars, because colliding O-star winds could also generate measurable X-ray fluxes (see Pittard & Stevens 1997) and the size of this cusp of stars can roughly account for the observed extent of CXOGC J174540.0−290027. The typical separation of these stars is about $0\farcs1$ or $\sim 10^{16}$ cm. Calculations by Pittard & Stevens indicate that a separation $\lesssim 10^{14}$ cm is needed, even in the most favorable case, to reproduce the observed luminosity of CXOGC J174540.0−290027. Therefore, one must again invoke close binary systems or expect only rare and brief events. Nothing is currently known concerning the binarity of these stars, but the dynamical evolution of binary systems should be relatively rapid in this dense stellar environment (see below). We note that the observed spectra of the O+O wind binaries HD 57060 and δ Orionis, which Pittard & Stevens compare to their models, have $kT < 1$ keV and would be unobservable at the Galactic center.

One may also consider an origin from young lower mass stars that may be present in the cluster. Late-type stars have X-ray emission elevated by factors of 10^1–10^4 above their main-sequence levels during their first 10^7 yr as a result of enhanced magnetic activity (Feigelson & Montmerle 1999). In two observed cases, X-ray flares exhibited peak $L_X \simeq (1\text{–}2) \times 10^{33}$ ergs s^{-1}, with $kT \simeq 7$–10 keV, and decays on timescales of hours (Preibisch, Neuhäuser, & Alcalá 1995; Tsuboi et al. 1998). It is thus possible that the rapid variation at the beginning of the observation originated in a young star rather than the SMBH. The quiescent X-ray emission from such stars does not exceed $L_X \sim 10^{31}$ ergs s^{-1}, however, so a population of $\sim 10^2$–10^3 magnetically active lower mass stars would be needed to produce all of the emission at Sgr A*. There are over a dozen O-type stars in the central $0\farcs5$ cusp. If we were to use the standard initial mass function (IMF) for stars in the solar neighborhood, we would expect there to be about 100 magnetically active low-mass stars per O star, so their combined luminosity would be $L_X \sim 10^{33}$–10^{34} ergs s^{-1}. It is believed, however, that the environment in the central parsec favors formation of higher mass stars and that the initial mass function in the central parsec may be flatter and may have a higher low-mass cutoff than in the solar neighborhood (Morris 1993). Dynamical mass segregation may also have worked to exclude low-mass stars from the central ≈ 0.01 pc.

The final stellar possibility that we consider for producing some fraction of the X-rays is that of a population of compact stellar objects in the entourage of the central black hole (Morris 1993; Lee 1995; Miralda-Escudé & Gould 2000). If the massive stars now observed in the central parsec evolve to produce stellar-mass black holes, and if those black holes are more massive than the bulk of the field stars in the stellar population of the central stellar core, then they will settle by gravitational segregation into a tight core comparable in size to the observed stellar distribution. If this process occurs in a quasi-continuous fashion over the lifetime of the Galaxy, then in the steady state a substantial number of stellar-mass black holes may be present in the compact central cluster, perhaps as many as 10^4–10^5. Interestingly, the collective luminosity of such a large number of compact objects, possibly including the most massive neutron stars, cannot compete with emission by a single object of the same total mass, because the Bondi accretion rate is proportional to the square of the accretor's mass (Bondi 1952). If a cluster of black holes is to contribute substantially to the X-ray emission, then it must contain close binaries with stellar companions that can contribute a substantial accretion flow.

Whether or not compact X-ray binaries exist in the cusp is a topic of considerable interest to stellar dynamicists. The velocity dispersion of stars in the cusp ($\gtrsim 100$ km s^{-1}) is at least an order of magnitude larger than in globular clusters (~ 10 km s^{-1}), so the favored mechanisms for forming binaries in globular clusters do not work in the stellar cusp at the center of our Galaxy (F. Rasio 2001, private communication; see also Rasio 1993). Rough estimates based on the tidal capture rate from hyperbolic orbits near the SMBH (Alexander & Kumar 2001; T. Alexander 2001, private communication) indicate that the number of X-ray binaries in the cusp at any given time should be at least 3 orders of magnitude below unity. Furthermore, frequent collisions with surrounding stars would cause any binaries to harden rapidly, leading either to disruption of the main-sequence star or to formation of short-lived common-envelope systems. In either case, the lifetimes of binaries in the cusp would probably be relatively brief.

In summary, the X-ray luminosity and spectrum of the source at Sgr A* are not extremely different from those seen in colliding-wind W-R binaries, but the absence of any He I star coincident with the X-ray source casts doubt on the presence of an appropriate binary at the correct location. The possible presence of one or more O+O binaries in the central stellar cusp cannot be excluded, but it seems doubtful that their spectra would be sufficiently hard. A population of young, magnetically active low-mass stars in the central stellar cusp could produce the observed luminosity and spectrum, but there is no observational evidence at this time that such low-mass stars are actually present in the required numbers. A population of 10^4–10^5 compact stellar-mass objects accreting hydrodynamically from the ambient medium could be present in the cusp, but their combined luminosity would be many orders of magnitude fainter than that of a single $\sim 10^6\ M_\odot$ black hole. An origin in an accreting X-ray binary system cannot be entirely excluded, but it seems improbable, owing to the difficulty of forming binaries in a stellar environment with such a high velocity dispersion and to the rapid dynamical evolution that would be expected for any binaries that might be formed. All things considered, a stellar origin for the bulk of the emission within $1\farcs5$ of Sgr A* is unlikely, and we proceed with the discussion assuming that the emission originates from accretion onto the SMBH.

9. SMBH ACCRETION AND X-RAY EMISSION MODELS

Assuming that the emission from CXOGC J174540.0−290027 is generated by matter accreting onto the supermassive black hole associated with Sgr A*, we can use the measured X-ray luminosity and spectrum to test various accretion and emission models for this source. As discussed in § 1, one would expect Sgr A* to emit $L_X \sim 3 \times 10^{43}$ ergs s^{-1} in the 2–10 keV band if it were radiating at the Eddington rate, whereas the observed luminosity reported in this paper is $\sim 10^{10}$ times fainter than that. Some fraction of the observed emission could be contributed by stellar objects within $\approx 1''$ of Sgr A*, so the true ratio could be even smaller. Sgr A* is thought to accrete matter from the stellar winds of nearby massive stars, particularly the He I stars in the central parsec cluster. Current estimates for the Bondi capture rate range from $\sim 3 \times 10^{-5}\ M_\odot$ yr^{-1} (Quataert et al.1999b) to $\sim 2 \times 10^{-4}\ M_\odot$ yr^{-1} (Coker & Melia 1997). Even at these rates, Sgr A* is underluminous in X-rays by factors of $\sim 10^7$–10^8 compared to the standard thin accretion disk model.

9.1. *Thermal Bremsstrahlung*

9.1.1. *Spectral Shape*

The low luminosity of Sgr A* may be explained either by accretion at a rate far below the estimated Bondi rate, by accretion at the Bondi rate of gas that is radiating very inefficiently, or by some combination of the two. Since there appears to be an ample supply of matter available from the stellar winds, research has concentrated on the study of low radiative efficiency accretion flows. Two prominent models developed over the past decade are the Bondi accretion and the ADAF models. Both of these models assume quasi-spherical infall onto the SMBH.

In the Bondi model (Melia 1992, 1994), the highly supersonic stellar winds flowing past Sgr A* form a bow shock that dissipates the bulk motion of the gas and heats it to a temperature of $\sim 10^7$ K. The ionized gas is then assumed to free-fall radially with no net angular momentum until it reaches the circularization radius at $R \sim 100 R_S$, where R_S is the Schwarzschild radius of the SMBH. Gravitational binding energy released during infall is transferred to the compressed magnetic field, which heats the ionized gas through some combination of magnetosonic and/or magnetoturbulent processes. Plasma microinstabilities and collective effects are then invoked to set up thermal equilibrium between the electrons and ions on a timescale shorter than the infall timescale. The ionized gas within the Keplerian region is assumed to infall on a timescale much shorter than the cooling time; consequently the thermal energy stored in the gas is lost as the gas crosses the event horizon of the SMBH.

In the ADAF models (Ichimaru 1977; Rees et al. 1982; Narayan, Yi, & Mahadevan 1995; Abramowicz et al. 1995; Mahadevan 1998), the gas is assumed to accrete with angular momentum. Turbulent magnetic viscosity dissipates energy and transfers angular momentum outward through the flow, allowing the accreting material to move inward. The bulk of the viscous energy is assumed to be deposited in the ions, with only a small fraction of the energy transmitted directly to the electrons. It is further assumed that electrons and ions interact only via the Coulomb process. The ions, mainly protons, are unable to radiate efficiently and maintain a temperature T_i close to the virial temperature at all radii ($T_i \sim 10^{12}/r$ K, where $r = R/R_S$). The electrons, on the other hand, radiate effectively via thermal bremsstrahlung at larger radii and also via synchrotron and Compton processes nearer the SMBH. At large radii, Coulomb scattering keeps the electrons and ions at a common temperature, but at smaller radii the relaxation timescale is longer than the infall timescale, so their temperatures diverge. The electron temperature begins to saturate at $\sim 10^3 R_S$, reaching a maximum of $\sim 10^9$–10^{10} K near the SMBH. Thus, a two-temperature plasma develops in the flow with the ions advecting the bulk of the released binding energy through the event horizon.

The "standard" Bondi and ADAF models described above assume the X-ray emission from Sgr A* is dominated by thermal bremsstrahlung emission from electrons in a hot, optically thin accretion flow. For both models, the predicted intrinsic spectrum in the *Chandra* band (0.1–10 keV) has photon index $\Gamma \sim 1.4$ (Melia 1994; Coker & Melia 2000; Narayan et al. 1998a). In the Bondi model, however, the bulk of the emission arises from a region within the circularization radius ($\lesssim 100 R_S$), while in the ADAF model the spectrum is dominated by emission from cooler gas at large radii ($\gtrsim 10^4 R_S$). This difference in the location of the dominant emitting region may be significant, as discussed below.

The best-fit, absorbed power-law model to the *Chandra* spectrum has $\Gamma = 2.7^{+1.3}_{-0.9}$, which is much steeper than the predicted spectrum for either model in the literature. Interestingly, the predicted photon index for both models lies near the lower limit of the 90% confidence interval, even after adjusting for the systematic effects discussed in § 5.3.1. The low luminosity and steep spectrum measured with *Chandra* imply that substantial modifications to the standard Bondi and ADAF models are needed, unless the accretion rate from the stellar winds is much lower than current estimates.

Recently, models have been developed in which not all the matter in the accretion flow at large radii makes its way to small radii and thence through the event horizon. The Bernoulli parameter in ADAF models is positive (Narayan & Yi 1994; Blandford & Begelman 1999), which means the gas accretes with positive energy and may escape. It is proposed that only a small fraction of the matter ($\sim 10^{-3}$) in the outer accretion flow makes it to the event horizon and that the binding energy released by this matter is transported to the outer parts of the flow, where it drives a substantial wind that carries off most of the matter. Hence, the amount of matter actually accreting through the event horizon is substantially reduced. Lowering the accretion rate at small radii would alleviate the need for the flow onto Sgr A* to have a radiative efficiency $\eta_r \lesssim 10^{-7}$. This is a very appealing concept, since such a low radiative efficiency would require that turbulent processes transfer energy from the protons to the electrons at an extremely low rate. As noted by Blandford & Begelman, their adiabatic inflow-outflow solutions (ADIOS) model generalizes the ADAF model to include the effects of a wind. Quataert & Narayan (1999a) have computed spectral models for Sgr A* using an ADAF+wind model.

ADAFs are thought to be unstable to convection for small values of the dimensionless viscosity parameter

$\alpha \lesssim 0.1$. This has given rise to convection-dominated accretion flow (CDAF) models (Ball, Narayan, & Quataert 2001; Quataert & Gruzinov 2000a), in which convection transfers angular momentum inward and energy outward through the flow. The inward transfer of angular momentum nearly cancels out the normal outward transfer, and the energy transported outward from the inner parts of the accretion flow heats the outer regions of the flow, retarding the rate of accretion. The net effect is that most of the matter circulates in convective eddies at large radii, rather than falling inward toward the event horizon. This excess matter eventually must be lost from the accretion flow in some manner, since otherwise a massive disk would build up over time.

One consequence of these new models is that the mass density distribution in the accretion flow rises less steeply toward the center. In the standard Bondi/ADAF models, the density ρ varies with radius R as $\rho(R) \propto R^{-3/2}$, while in the CDAF/ADAF+wind models $\rho \propto R^{-3/2+p}$. Here p is a variable used to parameterize the effect of a wind or convection on the density profile as a function of radius. Consequently, the accretion rate $\dot{M}$ is constant with radius in the Bondi/ADAF models, while in the CDAF/ADAF+wind models it varies with radius [$\dot{M}(R) \propto R^{-p}; 0 \leq p \leq 1$].

In the context of their ADAF+wind model, Quataert & Narayan (1999a) investigate the effect of wind strength on the spectrum. They find that, ignoring the weak frequency dependence of the Gaunt factor, the predicted spectrum in the *Chandra* band has photon index $\Gamma \approx 3/2 + 2p/\epsilon$, where $\epsilon \approx 1$ is the power-law index of the electron temperature profile ($T_e \propto R^{-\epsilon}$) in the outer parts of the flow. Comparing this to our measured spectrum of Sgr A*, we find that a modified ADAF model could be reconciled with the soft spectrum ($\Gamma \sim 2.7$) of Sgr A* if a substantial wind or strong convection ($p \approx 0.6$) is present.

Assuming that the observed X-ray spectrum is thermal bremsstrahlung from a hot accretion flow onto the SMBH and using the best-fit photon index, the predicted density profile through the flow would vary roughly as $R^{-0.9}$ in these models. The uncertainty in the measured photon index is too large to put tight constraints on the parameter p and hence on the density profile at this time; values of p in the range $\approx$0–1 are currently acceptable. Fortunately, useful constraints on the density profile are entirely feasible with *Chandra*/ACIS, given a long enough exposure.

There may be an additional complication, however, in using the observed spectrum to constrain the density profile of the accretion flow. Quataert (2002) argues that the observed spectral shape depends on the size of the telescope beam relative to the Bondi accretion radius. If the extended X-ray emission at Sgr A* comes from the accretion flow (§ 5.2), then the measured spectrum for a Bondi/ADAF flow may have a photon index significantly steeper than 1.4. If this argument is correct, then an accurate determination of the density profile would require a more sophisticated analysis than we have presented above.

9.1.2. *Accretion Rate and Emission Measure*

We use the properties of the hot gas surrounding Sgr A* to estimate the accretion rate at the Bondi capture radius (R_B) and to infer the accretion rate near the event horizon for the various hot accretion flow models discussed above. As reported in § 7, the best-estimate ambient plasma conditions are $n_e \approx 26\eta_f^{-1/2}$ cm^{-3} and $kT_e \approx 1.3$ keV.

The Bondi capture radius is given by the formula $R_B = 2GM/c_s^2$, where G is the gravitational constant, M is the mass of the black hole, and c_s is the speed of sound in the ambient plasma. The sound speed is given by the equation $c_s = (\gamma kT/\mu m_H)^{1/2} \approx 550$ km s^{-1}, which is comparable to the bulk velocities of the stellar winds ($\approx$200–1000 km s^{-1}; Paumard et al. 2001). Here γ is the adiabatic index, k is Boltzmann's constant, T and μ are the temperature and mean atomic weight of the gas, and m_H is the mass of a hydrogen atom. For simplicity, we assume that the process is adiabatic ($\gamma = 5/3$) and that the gas is fully ionized with twice solar abundances ($\mu \approx 0.70$). Inserting the value for the sound speed into the equation for the Bondi radius, we find that $R_B \approx 0.072$ pc (1.″8), comparable to the 1.″5 radius of the circle used to extract the spectrum. In the analysis to follow, we adopt $R_B = 0.06$ pc (1.″5 or $2.4 \times 10^5 R_S$) for the outer radius of the accretion flow.

Using the model of Bondi (1952), the accretion rate at R_B from a stationary plasma is then

$$\dot{M}_B = 4\pi\lambda(GM)^2\rho c_s^{-3} \simeq 1 \times 10^{-6}\left(\frac{n_e}{26\eta_f^{-1/2}\ \mathrm{cm}^{-3}}\right) \times \left(\frac{kT}{1.3\ \mathrm{keV}}\right)^{-3/2} M_\odot\ \mathrm{yr}^{-1}, \quad (1)$$

where $\lambda = \frac{1}{4}$ for an adiabatic process, and $\rho = n_e \mu m_H$ is the plasma density. This value for the accretion rate lies 1–2 orders of magnitude below the most recent estimates of the mass supply rate available from the stellar winds (see the discussion at the beginning of § 9). The accretion rate decreases if the local medium is moving past the SMBH at a rate $v_{local} \geq c_s$, roughly as $\dot{M}_B \propto (c_s^2 + v_{local}^2)^{-3/2}$.

The accretion rate for the standard ADAF model is related to the Bondi accretion rate by $\dot{M}_{ADAF} \sim \alpha \dot{M}_B$, where α is the dimensionless viscosity parameter in the standard thin accretion disk model (Shakura & Sunyaev 1973). Then

$$\dot{M}_{ADAF} \sim 1 \times 10^{-7}\left(\frac{\alpha}{0.1}\right)\left(\frac{n_e}{26\eta_f^{-1/2}\ \mathrm{cm}^{-3}}\right) \times \left(\frac{kT}{1.3\ \mathrm{keV}}\right)^{-3/2} M_\odot\ \mathrm{yr}^{-1} \quad (2)$$

throughout the accretion flow. For the ADIOS and CDAF models, the accretion rate scales with radius as $\dot{M}_{ADIOS/CDAF} \sim \alpha \dot{M}_B (R_S/R_B)^p$. Using $p = 0.6$ derived above from the *Chandra* spectrum of the source at Sgr A*, the predicted accretion rate across the event horizon would be

$$\dot{M}_{ADIOS} \sim 6 \times 10^{-11}\left(\frac{\alpha}{0.1}\right)\left(\frac{n_e}{26\eta_f^{-1/2}\ \mathrm{cm}^{-3}}\right) \times \left(\frac{kT}{1.3\ \mathrm{keV}}\right)^{-3/2} M_\odot\ \mathrm{yr}^{-1}. \quad (3)$$

In the CDAF model, the density profile is expected to be $\rho \propto R^{-1/2}$, so p should equal 1, which is within the uncertainties allowed by the *Chandra* spectrum. Thus, scaling the *Chandra* results using the CDAF model gives an accretion

rate at the event horizon of

$$\dot{M}_{\rm CDAF} \sim 4 \times 10^{-13} \left(\frac{\alpha}{0.1}\right) \left(\frac{n_e}{26\eta_f^{-1/2}\ {\rm cm}^{-3}}\right) \times \left(\frac{kT}{1.3\ {\rm keV}}\right)^{-3/2} M_\odot\ {\rm yr}^{-1}\ . \quad (4)$$

The rates predicted above for the ADIOS and CDAF models are valid only if the measured spectral slope does not depend strongly on the size of the telescope beam relative to the Bondi accretion radius (§ 9.1.1). Furthermore, these estimates are based solely on the properties of the hot gas surrounding Sgr A*; consequently, they do not account for any cold interstellar material that may be captured. Thus, the predicted accretion rate at $R_{\rm B}$ should be considered a lower limit on the true rate.

As noted in § 5.2, the X-ray emission at Sgr A* is extended on a scale consistent with the Bondi capture radius. If we assume that the quiescent emission from Sgr A* is dominated by bremsstrahlung emission from gas in the outer parts of the accretion flow, then we may use our best-fit, Raymond-Smith model (§ 5.3.1) to estimate the mean density ($n_e \approx 130\eta_f^{-1/2}$ cm^{-3}) and temperature ($kT_e \approx 2$ keV) of this gas. If we further assume that all the gas within the outer parts of the accretion flow has been heated by shocks, then these values indicate that the accretion rate at $R_{\rm B}$ given above should be increased by about a factor of 3. That is,

$$\dot{M}_{\rm B} \simeq 3 \times 10^{-6} \left(\frac{n_e}{130\eta_f^{-1/2}\ {\rm cm}^{-3}}\right) \times \left(\frac{kT}{2\ {\rm keV}}\right)^{-3/2} M_\odot\ {\rm yr}^{-1}\ . \quad (5)$$

Aitken et al. (2000) and Bower et al. (2003) report the detection of linearly polarized radio emission from Sgr A* at frequencies of 150 GHz and above (see § 2.1). Agol (2000) and Quataert & Gruzinov (2000b) show that this implies the Faraday rotation measure must be small and derive strong upper limits on the density and magnetic field strength at small radii in the accretion flow, where the polarized synchrotron emission is generated. Both groups assume an equipartition magnetic field and find that $\dot{M} \lesssim 10^{-8}\ M_\odot\ {\rm yr}^{-1}$ is required at small radii to prevent Faraday rotation from depolarizing the synchrotron emission. They propose that a CDAF or ADAF with an outflow could satisfy the conditions. The accretion-rate estimates derived above from our *Chandra* data indicate that either model could plausibly satisfy this requirement.

As mentioned above, the estimates derived for the hot gas may be lower limits on the total rate. Coker & Melia (1997) estimate the accretion rate from the stellar winds to be about $2 \times 10^{-4}\ M_\odot\ {\rm yr}^{-1}$, which is 200 times larger than the Bondi accretion rate for the hot gas. Scaling equations (3) and (4) by this amount reveals that ADIOS models with density profiles defined by the *Chandra* data (i.e., $p = 0.6$) would be marginally consistent with the upper limit on the accretion rate required by linear polarization, whereas CDAF models with flatter density profiles would be acceptable for all realistic wind accretion rates. Likewise, the magnetic field strength in Bondi models would have to be much weaker than equipartition to satisfy the observational constraints.

Theoretical studies of X-ray emission lines in hot accretion flows indicate that flows with strong winds should have stronger emission lines than flows with weak or no winds (Narayan & Raymond 1999; Perna, Raymond, & Narayan 2000). Narayan & Raymond estimate for Sgr A* that the equivalent width of Kα lines from He-like iron may range from about 180 eV (no wind) to about 1 keV (strong wind). This range lies well below our current upper limit of 2.2 keV (§ 5.3.2), so a sensitive search would require significantly more observing time with *Chandra*. Clearly, this would be a crucial observational test. The presence or absence of a 6.7 keV line in the Sgr A* spectrum would be a strong discriminant between thermal and nonthermal emission models, while the strength of the line, if present, would measure the strength of winds or convection in the accretion flow.

9.2. *Synchrotron Self-Compton*

Other prominent models for Sgr A* propose that the dominant X-ray emission mechanism is inverse Compton scattering of radio/millimeter synchrotron emission produced in the direct vicinity of the black hole. The primary distinctions between the various synchrotron self-Compton (SSC) models for Sgr A* lie in the location and properties of the relativistic electrons or pairs. Beckert & Duschl (1997) invoke a quasi-monoenergetic particle distribution in a static corona at $30R_{\rm S}$ or $40R_{\rm S}$ to account for the entire radio/mm spectrum and predict an SSC luminosity of 4×10^{33} ergs s^{-1}. Falcke & Markoff (2000) associate the X-ray flux with up-scattering of radio/millimeter emission generated in the nozzle of a jet with size $\lesssim 10R_{\rm S}$. In this model, the submillimeter bump in the radio spectrum is produced by relativistic electrons or pairs in the jet nozzle, while the flux at centimeter wavelengths comes from much larger distances in the jet, and the X-rays result from up-scattering of the submillimeter photons. Melia, Liu, & Coker (2001) similarly associate the X-ray flux with the submillimeter bump via the SSC process, but they model the synchrotron source as a hot, magnetized plasma in a Keplerian accretion disk at $\sim 5R_{\rm S}$, within the circularization radius of the accretion flow.

The SSC models predict that the X-ray flux is closely linked to one component of the radio/millimeter spectrum and that the two wavebands should vary in unison (Falcke & Markoff 2000; Melia, Liu, & Coker 2001). Thus, the large-amplitude temporal variations of the submillimeter component, observed on typical timescales of $\sim$20 days (Zhao, Bower, & Goss 2001), may set the timescale for, and would be correlated with, large-amplitude variations of the X-ray flux. In addition, X-ray variations of smaller amplitude may be associated with the many smaller scale variations that are seen on shorter timescales in the submillimeter band. The size of the emitting regions in these models indicate that significant variations may occur on timescales of a few hundred seconds or less.

The SSC models agree well with many of the X-ray results reported here. First, the 2–10 keV luminosity and power-law slope of both the Falcke & Markoff (2000) and Melia et al. (2001) models are quite consistent with the measured X-ray values. Interestingly, as these authors show, an electron Lorentz factor $\gamma_e \sim 100$ can produce both the correct submillimeter spectrum and the X-ray emission. Second, the SSC models are consistent with the evidence for an hour-long X-ray variation of up to a factor of 3 at the

beginning of the *Chandra* observation (§ 5.4.1). Third, these models generally require a much lower accretion rate than the estimated mass supply rate from stellar winds; the SSC models are thus more consistent with the detection of linear polarization in the radio band than are the standard Bondi and ADAF models. On the other hand, the SSC models predict that Sgr A* should be unresolved by the *Chandra* mirrors, whereas the X-ray emission at Sgr A* is clearly extended (§ 5.2).

There are a number of measurements that could be used to distinguish between the thermal bremsstrahlung and SSC emission models. First, the SSC models predict strongly correlated variability between the radio/millimeter and the X-ray bands, while the bremsstrahlung models do not. Second, X-rays from the SSC process should vary rapidly as a result of the proximity of the source region to the SMBH, while X-ray bremsstrahlung arising at larger radii should vary much more slowly. Third, the extended source that we have observed should appear more pointlike when it brightens if some of the X-rays are produced via the SSC mechanism near the MBH, while the more extended emission requires a thermal mechanism. Fourth, the quiescent X-ray spectrum should not show strong emission lines if it is dominated by the SSC mechanism, while the emission from the thermal model may show strong lines if significant convection or winds are present in the accretion flow. As discussed above, it is possible that both emission components may be present. In that case, analyses of changes in the morphology and spectrum of the source as it brightens and dims could be used to determine the relative strengths of the two components.

9.3. *Role of the Local Diffuse X-Ray Medium*

The models discussed in the previous sections are based on the assumption that the SMBH is accreting matter from the winds of nearby massive stars. However, it is conceivable that the SMBH is embedded in a hot X-ray–emitting gaseous region and not the cooler plasma ($\sim 10^4$ K) emerging from the stellar cluster.

It is evident from Figures 3–5 that hot plasma is prevalent throughout the central $\sim$10 pc of the Galaxy, and is concentrated with higher densities in the innermost $\sim$1 pc. This X-ray–emitting plasma will homogenize on timescales $l/c_s \lesssim 10^3$ yr, where $c_s \simeq 550$ km s^{-1} is the sound speed and $l \lesssim 1$ pc is the characteristic length scale of the inner region around Sgr A*. The morphology of the diffuse emission appears complex and is not symmetrical about Sgr A*, suggesting that it formed recently or is subject to external forces. This is supported by spectroscopic evidence that the local plasma is in a state of nonionization equilibrium (§ 7).

If the high surface brightness of the diffuse X-rays indicates the presence of a local, hot medium surrounding Sgr A*, then it could be the main source of material for accretion onto the SMBH. In this case, the accretion rate at R_B derived in § 9.1.2 would be a direct measurement of the mass supply rate at the capture radius, rather than a lower limit.

The relationships between the X-ray–emitting plasma seen in the ACIS images and other gaseous structures observed or inferred to be present are very unclear. First, the stellar winds from the massive OB/W-R stars in the cluster centered $\lesssim$0.1 pc from the SMBH may create a cavity of rapidly moving stellar gas within the hot ambient medium. This is the model discussed in most studies of Sgr A* accretion. The ram pressure of the winds is estimated to be about 2 orders of magnitude greater than the thermal pressure of the ambient medium and should dominate the ambient medium close to the stellar cluster. However, if the winds were to extend to very large distances without thermalizing to X-ray temperatures, the observed cusp in the diffuse X-ray emission should not be present. The spatial configuration of and the pressure balance between the cluster, SMBH, and ambient X-ray medium are thus not well established at the present time.

The relationships between the ambient X-ray plasma and other gaseous components in the Sgr A region are similarly unclear. First, as discussed in § 4 and by Maeda et al. (2002), the local plasma may have been recently compressed or pushed aside by the passage of the supernova shock wave of Sgr A East. Second, the hot medium may envelop the cooler spiral-shaped clouds of Sgr A West (see Fig. 4). If these clouds originated in the surrounding molecular ring, they are likely subject to heating and evaporation as they orbit inward toward the center.

At the present time, we are unable to determine whether the local diffuse X-ray–emitting medium does or does not affect the accretion onto the SMBH. However, future investigations of these issues must consider the hot ambient plasma, which is imaged at high spatial resolution for the first time in this study.

10. CONCLUSIONS

In this paper we have presented results of our first-epoch observation of the Galactic center performed with the ACIS-I instrument on the *Chandra X-ray Observatory*, which produced the first X-ray (0.5–7 keV) spectroscopic image with arcsecond resolution of the central $17' \times 17'$ (40 pc $\times$ 40 pc) of the Galaxy (§ 4). The image shows a bright ridge of diffuse X-ray emission running along the Galactic plane with the most intense emission coming from the vicinity of the Sgr A complex (see below).

Over 150 point sources are detected in the field: an increase in the X-ray source density at the Galactic center of more than an order of magnitude over that detected by previous X-ray satellites (§ 6). In the central parsec of the Galaxy, we have discovered a relatively strong X-ray source associated with the complex of stars in the luminous IR source IRS 13, and have tentatively identified a weaker X-ray source with the IR source AF NW. An apparent excess of X-rays just southwest of Sgr A* coincides within $\approx 1''$ with IRS 16SW, but the source is not detected by the wavelet algorithm that we used, perhaps because of its faintness and proximity to the relatively bright X-ray source located at the position of Sgr A*. Several X-ray sources in the central parsec have no corresponding IR source in the catalog of Ott et al. (1999). The brighter of these sources are likely candidates for new X-ray binaries.

A primary goal of this project is the search for an X-ray counterpart to Sgr A*, the compact nonthermal radio source associated with the 2.6×10^6 $M_\odot$ black hole at the dynamical center of the Galaxy. We have resolved the X-ray emission from the central parsec of the Galaxy and discovered a source, CXOGC J174540.0−290027, coincident with the radio position of Sgr A* to within $0\farcs27$, corresponding to a maximum projected distance of 12 lt-days (§ 5.1). The X-ray source has the following properties:

1. The 2–10 keV luminosity is $\simeq 2 \times 10^{33}$ ergs s^{-1}, assuming that the emission is isotropic (§ 5.3.1). This is $\sim 10^2$ times fainter than the upper limits obtained with previous X-ray satellites (§ 2.2) and $\sim 10^{10}$ times fainter than the X-ray luminosity predicted by the standard black hole thin accretion disk model if the source were radiating at the Eddington luminosity of the SMBH (§ 1).

2. The spectrum is well fitted either by an absorbed power law with photon index $\Gamma \approx 2.7$ or by an absorbed optically thin thermal plasma with $kT \approx 1.9$ keV (§ 5.3.1). In either case, the column density $N_{\rm H} \simeq 1 \times 10^{23}$ cm^{-2} is about twice the IR estimate. The spectrum is steeper than both the canonical AGN photon index ($\Gamma \simeq 1.5$–2.0) and the photon index ($\Gamma \simeq 1.4$) predicted by the "standard" Bondi and ADAF models (but see Quataert 2002). Here we have not included the effects of dust scattering in our spectral fits in order to remain consistent with models in the literature based on the results reported in an earlier version of this paper. Including dust scattering in the fits brings the column density into agreement with IR estimates but does not significantly affect the best-fit spectral slope (Baganoff et al. 2001). The systematic effects discussed in § 5.3.1 are more important.

3. The source is extended ($\gtrsim 11\ \sigma$ significance) with an intrinsic size $0\farcs61 \pm 0\farcs07$ that is consistent with the Bondi capture radius for the SMBH (§ 5.2).

4. A compact component within the source flared by up to a factor of 3 over a period of 3–4 ks at the start of the observation with $\gtrsim 99.34\%$ confidence (§ 5.4.1). The peak 2–10 keV luminosity of the flare was $\simeq 7 \times 10^{33}$ ergs s^{-1}.

5. A search for Kα line emission from iron was inconclusive (§ 5.3.2). The 90% confidence upper limit on the equivalent width is 2.2 keV.

Based on the fluxes and the spatial distribution of the X-ray sources in the field, we estimate that the probability of detecting an absorbed source by random chance that is as bright or brighter than the Sgr A* candidate and that lies within $0\farcs27$ of the radio position is $\lesssim 0.5\%$ (§ 5.1). As discussed in § 8, the nearest He stars are too far away ($\geq 1\farcs2$) to account for the X-ray source, and other classes of normal stars are too soft to penetrate the high absorbing column. Colliding winds in O+O binaries in the central stellar cusp may be able to produce the required luminosity, but their spectra might be too soft. A large population of young, magnetically active low-mass stars in the cusp could produce the observed luminosity and spectrum, but there is currently no evidence in the radio or IR bands that such stars are actually present. A population of 10^4–10^5 compact stellar-mass objects accreting hydrodynamically from the ambient medium appears an unlikely origin for the emission, since their cumulative luminosity would be many orders of magnitude fainter than that of a single $\sim 10^6\ M_\odot$ black hole. It is possible that the emission could originate in an accreting X-ray binary system within the cusp, but the expected number of X-ray binaries is $\lesssim 10^{-3}$.

Assuming that the observed emission within $1\farcs5$ of Sgr A* is from accretion onto the SMBH, we have used the observed properties of the source to constrain the models. Because of the limited photon statistics, the luminosity and spectral shape of the source can be fitted either by an optically thin thermal plasma model or by an SSC model. The measured extent of the source supports the thermal model, while the detection of rapid, large-amplitude variability supports the SSC model. The current observations, while of limited signal-to-noise ratio, are thus consistent with the presence of comparable levels of thermal and nonthermal emission in the Sgr A* spectrum.

The extremely low X-ray luminosity and steep spectrum that we have observed are very powerful constraints on all accretion and emission models for Sgr A*. In the case of SSC models, the luminosity and spectral slope constrain the magnetic field strength and Lorentz factor of electrons or pairs located in either a static plasma or a jet/outflow just outside the event horizon of the black hole. For thermal emission models, the constraints provide strong evidence that the "standard" Bondi and ADAF models must be modified. Bondi accretion models would need subequipartition magnetic fields, while ADAF models would need strong convection or outflows, unless the accretion rate from the stellar winds is much lower than anticipated. Even then, we estimate that the hot plasma surrounding Sgr A* should supply $\approx 10^{-6}\ M_\odot$ yr^{-1} at the Bondi radius, whereas the fact that Sgr A* is linearly polarized at 150 GHz and above limits the accretion rate near the event horizon to $\lesssim 10^{-8}\ M_\odot$ yr^{-1}, assuming an equipartition magnetic field. Thus, the X-ray and radio results together imply either that the rate of accretion decreases as material flows inward or that the magnetic field in the accretion flow is highly subequipartition.

Additionally, we have presented evidence that Sgr A* and Sgr A West are embedded in an NIE plasma extending across the central parsec of the Galaxy, with $kT \approx 1.3$ keV and $n_e \approx 26 \eta_f^{-1/2}$cm^{-3}, and that all three structures may lie within the ≈ 2 keV plasma in the central cavity of the shell-like nonthermal radio source Sgr A East, which we interpret as the remnant of a Type II supernova (§ 4). The morphology of the X-ray emission on the western side of the central parsec precisely matches 6 cm contours of the Western Arc of the Sgr A West minispiral, suggesting that the X-ray–emitting plasma may be confined by the CND in this direction. Alternatively, the similarity could result simply from line-of-sight absorption by the CND, but this would require a chance alignment in both space and time.

We propose here and in Maeda et al. (2002) that the X-ray luminosity of Sgr A* may have been significantly higher a few hundred years ago as the supernova blast wave swept through the position of the SMBH. Similarly, we have discovered bright clumps of X-ray emission located on opposite sides of the Galactic plane, along a line passing through the central parsec of the Galaxy. The arrangement of these lobes suggests that Sgr A* may have expelled hot gas in a bipolar outflow during an earlier period of increased activity lasting several thousand years.

This observation revealed two other remarkable extended X-ray features (§ 4): the source CXOGC J174544.4−285936 that we call "Sgr A Plume" and the source CXOGC J174540.3−290429 or XMM J174540−2904.5 that is associated with the radio structure called "Sgr A-E wisp" by Ho et al. (1985). Interestingly, both structures may be associated with supernova remnants, although their relative orientations are completely different. Ho et al. suggest that Sgr A-E wisp is the brightest part of a shell-like supernova remnant, while Sgr A Plume appears to extended directly into the heart of Sgr A East, at least in projection.

The results presented in this paper have demonstrated the potential of *Chandra*/ACIS to revolutionize our understanding of highly energetic phenomena in the central

parsec of our Galaxy. No other X-ray satellite for the foreseeable future will have its unique combination of arcsecond resolution, high sensitivity, broad energy band, and moderate spectral resolution. These properties are indispensable for this study. The results also show that further observations are needed to increase the photon statistics. An improved spectrum is needed to constrain the continuum shape and to search for line emission from He-like iron. Detection of such a line, for example, would show conclusively that a thermal component is present, while a nondetection would put tight constraints on the strength of a wind or outflow in the thermal models. The SSC models predict that the X-ray emission should be variable and should show a close correlation with variations in the millimeter band. A vigorous campaign of simultaneous monitoring in the X-ray and millimeter bands is needed to test this prediction. Likewise, increased photon statistics could be used to measure changes in the morphology and spectrum of the source as a function of energy and distance from the source. An order of magnitude longer exposure will be needed to achieve these goals.

We thank Farhad Yusef-Zadeh for the use of his VLA 6 cm image of Sgr A*; Peter Predehl for discussions regarding the *ROSAT* observations of Sgr A*; Heino Falcke, Fulvio Melia, and Eliot Quataert for explaining the similarities and differences between the various accretion flow and emission models; Rashid Sunyaev for sharing with us his physical insights into accretion flows and X-ray sources in the Galactic center; and Sabrina Pakzad for technical assistance with the identification of IR counterparts to X-ray sources. We especially thank the anonymous referee for providing many useful comments that improved this work. This research was supported by NASA grants NAS 8-38252 and NAS 8-00128. W. N. Brandt acknowledges support from NSF CAREER award AST 99-83783.

REFERENCES

Abramowicz, M. A., Chen, X., Kato, S., Lasota, J.-P., & Regev, O. 1995, ApJ, 438, L37
Agol, E. 2000, ApJ, 538, L121
Aitken, D. K., Greaves, J., Chrysostomou, A., Jenness, T., Holland, W., Hough, J. H., Pierce-Price, D., & Richer, J. 2000, ApJ, 534, L173
Alexander, T. 1999, ApJ, 527, 835
Alexander, T., & Kumar, P. 2001, ApJ, 549, 948
Anantharamaiah, K. R., Pedlar, A., Ekers, R. D., & Goss, W. M. 1991, MNRAS, 249, 262
Backer, D. C. 1996, in IAU Symp. 169, Unsolved Problems in the Milky Way, ed. L. Blitz & P. Teuben (Dordrecht: Kluwer), 193
Backer, D. C., & Sramek, R. A. 1999, ApJ, 524, 805
Backer, D. C., Zensus, J. A., Kellermann, K. I., Reid, M., Moran, J. M., & Lo, K. Y. 1993, Science, 262, 1414
Baganoff, F. 1999, ACIS On-Orbit Background Rates and Spectra from *Chandra* OAC Phase 1, ACIS Memo. 162, MIT Center for Space Research
Baganoff, F. K., et al. 2001, Nature, 413, 45
Balick, B., & Brown, R. L. 1974, ApJ, 194, 265
Ball, G. H., Narayan, R., & Quataert, E. 2001, ApJ, 552, 221
Beckert, T., & Duschl, W. J. 1997, A&A, 328, 95
Beckert, T., Duschl, W. J., Mezger, P. G., & Zylka, R. 1996, A&A, 307, 450
Becklin, E. E., Matthews, K., Neugebauer, G., & Willner, S. P. 1978, ApJ, 219, 121
Blandford, R. D., & Begelman, M. C. 1999, MNRAS, 303, L1
Blum, R. D., Sellgren, K., & DePoy, D. L. 1996, ApJ, 470, 864
Bondi, H. 1952, MNRAS, 112, 195
Bower, G. C., Backer, D. C., Zhao, J.-H., Goss, M., & Falcke, H. 1999a, ApJ, 521, 582
Bower, G. C., Falcke, H., & Backer, D. C. 1999b, ApJ, 523, L29
Bower, G. C., Falcke, H., Sault, R. J., & Backer, D. C. 2002, ApJ, 571, 843
Bower, G. C., Wright, M. C. H., Backer, D. C., & Falcke, H. 1999c, ApJ, 527, 851
Bower, G. C., Wright, M. C. H., Falcke, H., & Backer, D. C. 2001, ApJ, 555, L103
———. 2003, ApJ, 588, 331
Bradt, H. V. D., & McClintock, J. E. 1983, ARA&A, 21, 13
Coker, R. F., & Melia, F. 1997, ApJ, 488, L149
———. 2000, ApJ, 534, 723
Coker, R. F., Pittard, J. M., & Kastner, J. H. 2002, A&A, 383, 568
Corcoran, M. F. 1996, Rev. Mexicana Astron. Astrofis. Conf. Ser., 5, 54
Ebeling, H., White, D., & Rangarajan, V. 2001, MNRAS, submitted
Eckart, A., & Genzel, R. 1997, MNRAS, 284, 576
Eckart, A., Ott, T., & Genzel, R. 1999, A&A, 352, L22
Ekers, R. D., van Gorkom, J. H., Schwarz, U. J., & Goss, W. M. 1983, A&A, 122, 143
Eyles, C. J., Skinner, G. K., Willmore, A. P., & Rosenberg, F. D. 1975, Nature, 257, 291
Falcke, H. 1999, in ASP Conf. Ser. 186, The Central Parsecs of the Galaxy, ed. H. Falcke, A. Cotera, W. J. Duschl, F. Melia, & M. Rieke (San Francisco: ASP), 113
Falcke, H., & Markoff, S. 2000, A&A, 362, 113
Feigelson, E. D. 2001, in ASP Conf. Ser. 234, X-Ray Astronomy 2000, ed. R. Giacconi, L. Stella, & S. Serio (San Francisco: ASP), 131
Feigelson, E. D., & Montmerle, T. 1999, ARA&A, 37, 363
Frank, J., King, A., & Raine, D. 1992, Accretion Power in Astrophysics (2d ed.; Cambridge: Cambridge Univ. Press)
Freeman, P. E., Kashyap, V., Rosner, R., & Lamb, D. Q. 2002, ApJS, 138, 185
Garcia, M. R., Murray, S. S., Primini, F. A., Forman, W. R., McClintock, J. E., & Jones, C. 2000, ApJ, 537, L23
Gehrels, N. 1986, ApJ, 303, 336
Genzel, R., Eckart, A., Ott, T., & Eisenhauer, F. 1997, MNRAS, 291, 219
Genzel, R., Pichon, C., Eckart, A., Gerhard, O. E., & Ott, T. 2000, MNRAS, 317, 348
Genzel, R., Thatte, N., Krabbe, A., Kroker, H., & Tacconi-Garman, L. E. 1996, ApJ, 472, 153
Ghez, A. M., Klein, B. L., Morris, M., & Becklin, E. E. 1998, ApJ, 509, 678
Ghez, A. M., Morris, M., Becklin, E. E., Tanner, A., & Kremenek, T. 2000, Nature, 407, 349
Goldwurm, A., et al. 1994, Nature, 371, 589
Ho, L. C., et al. 2001, ApJ, 549, L51
Ho, P. T. P., Jackson, J. M., Barrett, A. H., & Armstrong, J. T. 1985, ApJ, 288, 575
Høg, E., et al. 2000, A&A, 355, L27
Ichimaru, S. 1977, ApJ, 214, 840
Jones, T. W. 1974, A&A, 30, 37
Kaastra, J. S. 1992, An X-Ray Spectral Code for Optically Thin Plasmas: Updated Version 2.0 (Leiden: SRON)
Kawai, N., Fenimore, E. E., Middleditch, J., Cruddace, R. G., Fritz, G. G., Snyder, W. A., & Ulmer, M. P. 1988, ApJ, 330, 130
Kennea, J. A., & Skinner, G. K. 1996, PASJ, 48, L117
Khokhlov, A., & Melia, F. 1996, ApJ, 457, L61
Koyama, K., Awaki, H., Kunieda, H., Takano, S., Tawara, Y., Yamauchi, S., Hatsukade, I., & Nagase, F. 1989, Nature, 339, 603
Koyama, K., Kawada, M., Takano, S., & Ikeuchi, S. 1990, PASJ, 42, L1
Koyama, K., Maeda, Y., Sonobe, T., Takeshima, T., Tanaka, Y., & Yamauchi, S. 1996, PASJ, 48, 249
Koyama, K., Maeda, Y., Tsuru, T., Nagase, F., & Skinner, S. 1994, PASJ, 46, L93
Krabbe, A., et al. 1995, ApJ, 447, L95
Kundt, W. 1990, Ap&SS, 172, 109
Lang, C. C., Morris, M., & Echevarria, L. 1999, ApJ, 526, 727
Lee, H. M. 1995, MNRAS, 272, 605
Lynden-Bell, D., & Rees, M. J. 1971, MNRAS, 152, 461
Maeda, Y., et al. 2002, ApJ, 570, 671
Maeda, Y., Koyama, K., Sakano, M., Takeshima, T., & Yamauchi, S. 1996, PASJ, 48, 417
Maeda, Y., Koyama, K., Yokogawa, J., & Skinner, S. 1999, ApJ, 510, 967
Mahadevan, R. 1998, Nature, 394, 651
Maoz, E. 1998, ApJ, 494, L181
Marr, J. M., Wright, M. C. H., & Backer, D. C. 1993, ApJ, 411, 667
Mayer-Hasselwander, H. A., et al. 1998, A&A, 335, 161
Melia, F. 1992, ApJ, 387, L25
———. 1994, ApJ, 426, 577
Melia, F., & Falcke, H. 2001, ARA&A, 39, 309
Melia, F., Liu, S., & Coker, R. 2001, ApJ, 553, 146
Menten, K. M., Reid, M. J., Eckart, A., & Genzel, R. 1997, ApJ, 475, L111
Mewe, R., Gronenschild, E. H. B. M., & van den Oord, G. H. J. 1985, A&AS, 62, 197
Mezger, P. G., et al. 1989, A&A, 209, 337
Miralda-Escudé, J., & Gould, A. 2000, ApJ, 545, 847
Morris, M. 1993, ApJ, 408, 496
Morris, M., & Serabyn, E. 1996, ARA&A, 34, 645

Morris, M., & Yusef-Zadeh, F. 1985, AJ, 90, 2511
Murakami, H., Koyama, K., Sakano, M., Tsujimoto, M., & Maeda, Y. 2000, ApJ, 534, 283
Murakami, H., Koyama, K., Tsujimoto, M., Maeda, Y., & Sakano, M. 2001, ApJ, 550, 297
Najarro, F., Krabbe, A., Genzel, R., Lutz, D., Kudritzki, R. P., & Hillier, D. J. 1997, A&A, 325, 700
Narayan, R., Mahadevan, R., Grindlay, J. E., Popham, R. G., & Gammie, C. 1998a, ApJ, 492, 554
Narayan, R., Mahadevan, R., & Quataert, E. 1998b, in Theory of Black Hole Accretion Disks, ed. M. A. Abramowicz, G. Bjornsson, & J. E. Pringle (Cambridge: Cambridge Univ. Press), 148
Narayan, R., & Raymond, J. 1999, ApJ, 515, L69
Narayan, R., & Yi, I. 1994, ApJ, 428, L13
Narayan, R., Yi, I., & Mahadevan, R. 1995, Nature, 374, 623
Ott, T., Eckart, A., & Genzel, R. 1999, ApJ, 523, 248
Ozernoy, L. M. 1989, in IAU Symp. 136, The Center of the Galaxy, ed. M. Morris (Dordrecht: Kluwer), 555
Ozernoy, L. M., Genzel, R., & Usov, V. V. 1997, MNRAS, 288, 237
Paumard, T., Maillard, J. P., Morris, M., & Rigaut, F. 2001, A&A, 366, 466
Pavlinsky, M. N., Grebenev, S. A., & Sunyaev, R. A. 1994, ApJ, 425, 110
Pedlar, A., Anantharamaiah, K. R., Ekers, R. D., Goss, W. M., van Gorkom, J. H., Schwarz, U. J., & Zhao, J.-H. 1989, ApJ, 342, 769
Perna, R., Raymond, J., & Narayan, R. 2000, ApJ, 541, 898
Pessah, M., & Melia, F. 2003, ApJ, 585, L29
Pittard, J. M., & Stevens, I. R. 1997, MNRAS, 292, 298
Predehl, P., & Schmitt, J. H. M. M. 1995, A&A, 293, 889
Predehl, P., & Trümper, J. 1994, A&A, 290, L29
Predehl, P., & Zinnecker, H. 1996, in ASP Conf. Ser. 102, The Galactic Center, ed. R. Gredel (San Francisco: ASP), 415
Preibisch, T., Neuhäuser, R., & Alcalá, J. M. 1995, A&A, 304, L13
Prigozhin, G., Kissel, S., Bautz, M., Grant, C., LaMarr, B., Foster, R., Ricker, G., & Garmire, G. 2000, Proc. SPIE, 4012, 720
Quataert, E. 2002, ApJ, 575, 855
Quataert, E., & Gruzinov, A. 2000a, ApJ, 539, 809
———. 2000b, ApJ, 545, 842
Quataert, E., & Narayan, R. 1999a, ApJ, 520, 298
Quataert, E., Narayan, R., & Reid, M. J. 1999b, ApJ, 517, 101
Rasio, F. A. 1993, PASP, 105, 973
Raymond, J. C., & Smith, B. W. 1977, ApJS, 35, 419
Rees, M. J., Begelman, M. C., Blandford, R. D., & Phinney, E. S. 1982, Nature, 295, 17
Reid, M. J. 1993, ARA&A, 31, 345
Reid, M. J., Readhead, A. C. S., Vermeulen, R. C., & Treuhaft, R. N. 1999, ApJ, 524, 816
Rieke, G. H., Rieke, M. J., & Paul, A. E. 1989, ApJ, 336, 752
Rogers, A. E. E., et al. 1994, ApJ, 434, L59
Sakano, M., Warwick, R. S., Decourchelle, A., & Predehl, P. 2003, MNRAS, 340, 747
Sault, R. J., & Macquart, J.-P. 1999, ApJ, 526, L85
Schödel, R., et al. 2002, Nature, 419, 694
Shakura, N. I., & Sunyaev, R. A. 1973, A&A, 24, 337
Sidoli, L., & Mereghetti, S. 1999, A&A, 349, L49
Sidoli, L., Mereghetti, S., Israel, G. L., Chiappetti, L., Treves, A., & Orlandini, M. 1999, ApJ, 525, 215
Skinner, G. K. 1989, in IAU Symp. 136, The Center of the Galaxy, ed. M. Morris (Dordrecht: Kluwer), 567
Skinner, G. K., et al. 1987, Nature, 330, 544
Stolovy, S. R., Hayward, T. L., & Herter, T. 1996, ApJ, 470, L45
Sunyaev, R. A., Markevitch, M., & Pavlinsky, M. 1993, ApJ, 407, 606
Terashima, Y., Ho, L. C., & Ptak, A. F. 2000, ApJ, 539, 161
Tsuboi, Y., Koyama, K., Murakami, H., Hayashi, M., Skinner, S., & Ueno, S. 1998, ApJ, 503, 894
Tsuboi, M., Miyazaki, A., & Tsutsumi, T. 1999, in ASP Conf. Ser. 186, The Central Parsecs of the Galaxy, ed. H. Falcke, A. Cotera, W. J. Duschl, F. Melia, & M. Rieke (San Francisco: ASP), 105
Wang, Q. D., Gotthelf, E. V., & Lang, C. C. 2002, Nature, 415, 148
Watson, M. G., Willingale, R., Grindlay, J. E., & Hertz, P. 1981, ApJ, 250, 142
Weisskopf, M. C., O'dell, S., & van Speybroeck, L. P. 1996, Proc. SPIE, 2805, 2
Williams, P. M., van der Hucht, K. A., Pollock, A. M. T., Florkowski, D. R., van der Woerd, H., & Wamsteker, W. M. 1990, MNRAS, 243, 662
Wright, M. C. H., & Backer, D. C. 1993, ApJ, 417, 560
Wright, M. C. H., Coil, A. L., McGary, R. S., Ho, P. T. P., & Harris, A. I. 2001, ApJ, 551, 254
Wright, M. C. H., Genzel, R., Güsten, R., & Jaffe, D. T. 1987, in AIP Conf. Proc. 155, The Galactic Center, ed. D. C. Backer (New York: AIP), 133
Yusef-Zadeh, F., Melia, F., & Wardle, M. 2000, Science, 287, 85
Yusef-Zadeh, F., & Morris, M. 1987, ApJ, 320, 545
Zhao, J.-H., Bower, G. C., & Goss, W. M. 2001, ApJ, 547, L29
Zhao, J., Ekers, R. D., Goss, W. M., Lo, K. Y., & Narayan, R. 1989, in IAU Symp. 136, The Center of the Galaxy, ed. M. Morris (Dordrecht: Kluwer), 535